REV 1

Dissolution-reprecipitation versus solid-state diffusion: mechanism of mineral transformations in sylvanite, $(AuAg)_2Te_4$, under hydrothermal conditions

Jing Zhao[1,2], Joël Brugger[2,3], Fang Xia[2,3], Yung Ngothai[1], Guorong Chen[4], and Allan Pring[2,3]*

[1]School of Chemical Engineering, University of Adelaide, Adelaide, SA 5005, Australia

[2]Department of Mineralogy, South Australian Museum, North Terrace, Adelaide, SA 5000, Australia

[3]Tectonics, Resources and Exploration (TRaX), School of Earth and Environmental Sciences, University of Adelaide, Adelaide, SA 5005, Australia

[4]Key Laboratory for Ultrafine Materials of Ministry of Education, School of Materials Science and Engineering, East China University of Science and Technology, Shanghai 200237, China

*Corresponding author: E-mail: allan.pring@samuseum.sa.gov.au

Always consult and cite the final, published document. See http://www.minsocam.org or GeoscienceWorld

Abstract

Under hydrothermal conditions, diffusion-driven solid-state reactions can compete with fluid-mediated reaction mechanisms. We obtained an insight into the complex textures resulting from such competition by studying experimentally the transformation of the Au-Ag-telluride sylvanite to Au-Ag alloy under hydrothermal conditions, and probing the effects of temperature (160-220 ˚C), pH (2-10), and redox conditions on the sample textures and the reaction kinetics. Sylvanite transformed to Au-Ag alloy over all hydrothermal conditions explored, but not under dry conditions. The replacement was pseudomorphic, as Au-Ag alloy preserved the external dimensions of the sylvanite grains. The resulting Au-Ag alloy was porous, consisting of worm-like aggregates with diameters ranging from 200 nm to 1 μm. In addition to Au-Ag alloy, a range of other phases were observed as intermediate products, including petzite (Ag_3AuTe_2), hessite (Ag_2Te), and two compositions of calaverite: an Ag-rich-Te-depleted composition, $(Au_{0.78}Ag_{0.22})Te_{1.74}$, and a normal calaverite, $(Au_{0.93}Ag_{0.07})Te_2$.

The transformation of sylvanite to Au-Ag alloy follows a complex reaction path, with competing reactions proceeding either via interface-coupled dissolution and reprecipitation (ICDR) mechanism or via solid-state exsolution. Initially, sylvanite was replaced by Au-Ag alloy following an ICDR mechanism, with sylvanite dissolution being rate-limiting relative to Au-Ag alloy precipitation. Tellurium was lost to the bulk solution as tellurite or telluride complexes, depending on redox conditions. Once the concentration of tellurium in solution reached a critical state, the reaction switched and sylvanite dissolution was coupled to the precipitation of an Ag-rich-Te-depleted calaverite. This Ag-rich-Te-depleted calaverite decomposes via exsolution to calaverite and phase *X* ($Ag_{3+x}Au_{1-x}Te_2$ with $0.1 < x < 0.55$),

Always consult and cite the final, published document. See http://www.minsocam.org or GeoscienceWorld

which in turn breaks down to a mixture of low petzite and low hessite below 120 ˚C via exsolution. As the reaction continues, the calaverite and phase *X* are all transformed to Au-Ag alloy via ICDR. In the ICDR reactions the Au-Ag alloy precipitated locally near the telluride dissolution site. Such local Au-Ag alloy precipitation is facilitated by fast heterogeneous nucleation onto the sylvanite, calaverite and petzite surfaces. The dissolution of sylvanite and of the intermediate telluride species, and the overall reaction, are oxidation reactions. The diffusion of oxygen through the porous Au-Ag alloy layer plays an important role in sustaining the reaction.

A similar combination of dissolution-reprecipitation and solid-state processes may be responsible for the formation of some of the Au and Au-Ag telluride assemblages observed in Nature. These processes may also play a role in the formation of mineral assemblages in Cu-Fe sulfide systems, where the solid-state mobility of Cu^{+} ions is relatively high at moderate temperatures. The interplay of different reaction mechanisms results in complex textures, which could easily be misinterpreted in terms of complex geological evolution. At 220 ˚C, solid-state replacement of sylvanite by Au-Ag alloy is slow (months), but under hydrothermal conditions sylvanite grains ~100 μm in size can be fully replaced in as little as 96 hours, providing a possible alternative to roasting as a pre-treatment of telluride-rich gold ores.

Keywords: sylvanite, gold, dissolution-reprecipitation, exsolution, pseudomorphism, replacement, reaction mechanism, texture.

Always consult and cite the final, published document. See http://www.minsocam.org or GeoscienceWorld

Introduction

The importance of interface-coupled dissolution reprecipitation (ICDR) reactions in a wide variety of geological processes is becoming widely recognized (Putnis 2002, 2009), and this is particularly so in ore deposition and enrichment (Tenailleau et al. 2006; Xia et al. 2007, 2008, 2009; Qian et al. 2010, 2011; Tooth et al. 2011). In the chalcogenide systems studied to date, the temperatures of the reactions were such that the mobility of the metal ions, due to self-diffusion, was low. So in these reactions the kinetics of any solid-state, diffusion-driven process was likely to be very sluggish when compared to the kinetics of ICDR reactions. It is clear, however, that in higher temperature settings such as porphyry copper systems or intrusion-related gold deposits, solid-state diffusion may be significant, and solid-state reactions may compete kinetically with the ICDR mechanism. The same consideration applies to more mobile chalcogenide systems such as some Ag and Cu sulfides, selenides and tellurides.

Gold and Au-Ag tellurides are important accessory minerals in many gold deposits, and in some deposits they carry a significant proportion of the Au (Cook 2009). Recently Zhao et al. (2009, 2010) showed that calaverite, $AuTe_2$, can be transformed to gold over a wide range of hydrothermal conditions. At temperatures above 200 ˚C the transformation takes place in the laboratory on < 1mm grains in 24 to 48 h but is limited by the solubility of Te(IV) in the solution. The transformation proceeds in pseudomorphic manner via a coupled calaverite dissolution – gold precipitation mechanism, with calaverite dissolution being rate-limiting relative to gold precipitation. Tellurium is lost to the bulk solution as Te(IV) complexes, and may precipitate away from the dissolution site as TeO_2(s). In contrast, gold precipitates locally near the calaverite dissolution site. Such local gold

Always consult and cite the final, published document. See http://www.minsocam.org or GeoscienceWorld

precipitation is facilitated by fast heterogeneous nucleation onto the calaverite surface. The dissolution of calaverite and the overall reaction are oxidation reactions, and oxygen diffusion through the porous metallic gold layer probably plays an important role in sustaining the reaction. The porous gold produced by these reaction mechanisms has porosity on the scale of 0.1 to 1 μm.

Sylvanite, $AuAgTe_4$, and petzite, Ag_3AuTe_2, are also important Au-Ag telluride minerals and are found principally in low-temperature hydrothermal vein deposits (≤200 ˚C), for example the Emperor deposit, Fiji, where sylvanite is the most common telluride (Pals and Spry 2003). Sylvanite and petzite are often associated in Nature and found with native tellurium, gold, quartz, calaverite, and other rare telluride minerals. Chemically, sylvanite is a Au-Ag telluride. The ratio between Au and Ag varies from 3:1 to 1:1. Sylvanite crystallizes in the monoclinic *P*2/*c* space group and the subcell is a = 8.96 Å, b = 4.49 Å, c = 14.62 Å, β = 145.433 ° (Pertlik 1984). The structure of sylvanite consists of distorted $AgTe_6$ (2 + 2 + 2 coordination) and $AuTe_6$ (4 + 2 coordination) octahedra sharing edges to form continuous brucite-like sheets // (100); the sheets are linked into a framework by relatively short Te-Te bonds (2.823 Å). The structure topology of sylvanite is similar to that of calaverite, a monoclinic mineral with a unit cell of a = 7.19 Å, b = 4.41 Å, c = 5.07 Å, β = 90 ° and the space group *C*2/*m* or *I*2 (Schutte and de Boer 1988; Strunz and Nickel 2001). In calaverite, the $AuTe_6$ octahedral layers are //(001), the Au coordination is 2 + 4 (rather than 4 + 2 in sylvanite), and the Te-Te bonds linking the layers are bifurcating and longer than in sylvanite (3.192 versus 2.823 Å). Sylvanite melts at 354 ˚C and it has been suggested that the mineral undergoes a high-low phase transition but details are sketchy (Cabri 1965; Vaughan and Craig 1978).

Always consult and cite the final, published document. See http://www.minsocam.org or GeoscienceWorld

Petzite, a metal-rich telluride mineral compared to calaverite and sylvanite, has a garnet-like structure (cubic symmetry, $I4_132$) consisting of edge-sharing $Ag[Te_4Ag_2Au_2]$ and $Au[Ag_6Te_2]$ polyhedra (Strunz and Nickel 2001; Reithmayer 1993). It has been reported that petzite undergoes a phase transition to intermediate and low temperature forms but data on the structural changes and the temperature of transition are limited (Cabri 1965; Vaughan and Craig 1978). Recent detailed studies on tellurides in the Kalgoorlie district by Shackleton et al. (2003) reported mineral assemblages of calaverite-sylvanite, sylvanite-hessite and sylvanite-petzite-hessite. Based on textural evidence and calculated stability diagrams, it has been proposed that the formation of these mineral assemblages is the result of mineral replacement reactions under hydrothermal conditions (Shackleton et al. 2003).

Here we present the results of a laboratory study into the transformation of sylvanite to gold (strictly speaking, a Au-Ag alloy) over a range of hydrothermal conditions. Given that sylvanite melts at 354 ˚C it is reasonable to expect that cation diffusion in this mineral will be significant at temperatures above 145 ˚C (two thirds of the melting point in kelvin) for experiments on a laboratory time scale (days to months). One aim of this work is to establish the mechanism of mineral replacement of an Au-Ag telluride, to characterize the resulting textures, and to compare these results to our previous studies on the replacement of calaverite (Zhao et al. 2009, 2010). In particular we were interested to track the fate of the Ag during the transformation and to assess whether solid-state diffusions processes interact with dissolution-reprecipitation processes in this system.

Always consult and cite the final, published document. See http://www.minsocam.org or GeoscienceWorld

Samples and methods

Preparation of natural samples

Crystals of sylvanite from Vatukoula, Tavua Goldfield, Vitei Levu, Fiji (SA Museum specimen G31671 and Museum Victoria E16799), of average composition $Au_{1.26}Ag_{0.71}Sb_{0.03}Te_{4.00}$, were used throughout this study. The identification of the sylvanite was confirmed by powder X-ray diffraction and the composition determined by electron probe microanalysis. SEM imaging revealed that some crystals contain a small number of 1 to 5 μm inclusions of euhedral calaverite crystals. These calaverite inclusions appear to have a consistent crystallographic relationship to the host sylvanite, but were too small to be successfully investigated by electron backscatter diffraction. The sylvanite crystals were crushed and sieved, and the size fraction 150-400 μm was used in the hydrothermal experiments so as to have a constant mass to surface area ratio.

Preparation of buffer solutions

Milli-Q water (conductivity of 18 MΩ cm^{-1}; Direct-Q3 system, Millipore corp.) and three buffer solutions of different pHs were used to study the effect of pH on the reaction mechanism and kinetics. Buffer solutions with $pH_{25\,^{\circ}C}$ 2, 7 and 10 were prepared (Table 1) using Milli-Q water at room temperature (~ 25 ˚C). These solutions also contained 0.01 *M* NaCl, in order to more closely mimic natural hydrothermal waters and provide a ligand for increasing Ag mobility. A temperature-corrected pH-meter (EUTECH Scientific, model Cyber-scan 510) with an Ag/AgCl pH electrode was used for the pH measurements. Calibrations were performed with AQUASPEX standard buffer solutions: $pH_{25\,^{\circ}C}$ = 4.01 (KH-phthalate buffer), $pH_{25\,^{\circ}C}$ = 7.00 (phosphate buffer), and $pH_{25\,^{\circ}C}$ = 10.01 (carbonate

Always consult and cite the final, published document. See http://www.minsocam.org or GeoscienceWorld

153 buffer). The pHs the of buffer solutions at reaction temperature were calculated using
154 Geochemist's Work Bench (GWB), and $pH_{220\ ^\circ C}$ are listed in Table 1.

155 **Hydrothermal experiments**

156 The hydrothermal experiments were conducted using 25 mL Teflon cells sealed in stainless
157 steel autoclaves. Typically, 10 mg of sylvanite crystal fragments and 15 mL of reaction
158 solution were added to the cell, leaving a 10 mL headspace for expansion. Hydrothermal
159 experiments (Table 2) were performed in electric muffle furnaces or ovens (both with a
160 temperature regulation precision of ± 2 ˚C) at 160 ˚C (Runs D1-D4), 190 ˚C (Runs C1-C7)
161 or 220 ˚C (runs A1-28, B1-B11, E1-E3, F1-F4) at autogenous pressures (< 20 bar). The
162 redox conditions were also varied. In experimental runs A1- A28, the amount of O_2 in the
163 system was controlled by the air in the headspace. To increase the amount of O_2(aq) in the
164 system, 20 µL of 30 wt% H_2O_2 solution were added to the cells; above 80 ˚C H_2O_2
165 decomposes to give O_2(aq) (runs B1-B11). To obtain reducing environments, the
166 headspace of the cell above the solution was filled with 1% H_2 in Ar mixture in a glove box
167 prior sealing the autoclave (experiments F1-F4).

168 After reaction, the autoclaves were rapidly cooled by quenching in a large volume of cold
169 water (~10 L) for 30 minutes. The reacted fluid was collected after the autoclaves were
170 opened, and solids were rinsed three times with Milli-Q water and then three times with
171 acetone before drying. Results from leaking runs were discarded.

172 **Solid-state diffusion (dry runs)**

173 The solid-state transformation experiments (Table 3) were carried out by heating sylvanite
174 grains at 220 ˚C in both unsealed (runs G1-G3) and sealed evacuated quartz glass tubes

Always consult and cite the final, published document. See http://www.minsocam.org or GeoscienceWorld

(H1-H3) in a muffle furnace for periods of 24, 48 and 1344 hours. Following that, the furnace was turned off and the samples were allowed to cool in the furnace to room temperature.

X-ray Diffraction (XRD)

Room-temperature powder X-ray diffraction (XRD) patterns of the samples were collected using a Huber Guinier Image Plate G670 with $CoK\alpha_1$ radiation (λ = 1.78892 Å). The specimens were ground under acetone in an agate mortar and spread on a Mylar film. Powder diffraction data was collected for 20 min or recollected for longer periods to obtain >2000 counts intensity for the strongest peak in each pattern. The extent of the transformation was determined by the Rietveld quantitative phase analysis method (QPA) using the program Rietica (Rietveld 1969; Hunter 1998). Diffraction data in the 2θ range from 20 to 80 ° was used in the QPA. A Pseudo-Voigt function with Howard asymmetry (Howard 1982) and Shifted Cheby II function were adopted to model the peak shapes and the background, respectively. Zero shifts were taken from refinements of NBS internal Si standard. The refined parameters include: the scale factor (S), background, cell parameters and the peak-shape parameters (U, V, W). For each run, the reaction extent, y, was calculated as $y = 1 - y_{(sylvanite)}$, where $y_{(sylvanite)}$ is the mole fraction of sylvanite among the products as determined by QPA.

Scanning Electron Microscopy (SEM)

A Philips XL30 field emission scanning electron microscope (FESEM) at Adelaide Microscopy, University of Adelaide, was used for characterization of the morphological and textural features of the grains. The FESEM was operated at 20 kV. Secondary Electron (SE) imaging was used to characterize the surface morphology of the grains before and

Always consult and cite the final, published document. See http://www.minsocam.org or GeoscienceWorld

after the reaction. For textural studies, samples were embedded in epoxy resin, sectioned and polished (down to 1 μm diamond paste) and evaporatively coated with 15 nm thick carbon films. The polished cross sections were examined in Back Scattered Electron (BSE) mode and also by reflected light optical microscopy.

Electron backscatter diffraction (EBSD)

EBSD pole figures, used to establish the relative crystallographic orientations of sylvanite and products phases, were collected using a HKL EBSD system fitted in the Philips XL30 FESEM at Adelaide Microscopy. The samples were first polished with diamond paste (3 and 1 μm) for 20 min, and then polished with 0.04 μm colloidal silica suspension for 60 min to attempt to remove the damaged layer. After polishing, the samples were coated with a 1.5 nm thick carbon film to minimize charging. The EBSD analyses were performed with the polished sample surface tilted 70 ° relative to the horizontal and with a 20 kV accelerating voltage, 0.6 nA specimen current, and a working distance of 20 mm. The EBSD patterns were recorded using a Nordlys camera. The HKL Channel 5 and MTEX (Bachmann et al. 2010) software packages were used for data collection and interpretation, respectively. Crystal structural data for sylvanite, calaverite and gold were from the ICSD database (sylvanite code: 24646; calaverite code: 64681; gold code: 44362).

Chemical analysis of solid products

The chemical compositions of the sylvanite and reaction products were determined by electron probe microanalysis in WDS mode using a Cameca SX-51 instrument at Adelaide Microscopy, University of Adelaide, operated at an accelerating voltage of 20 kV and a beam current of 20 nA. The following standards were used: Au (Au), Bi_2Se_3 (Bi, Se), PbS (Pb, S), Ag_2Te (Ag, Te), Sb_2S_3 (Sb), CoAsS and GaAs (As).

Always consult and cite the final, published document. See http://www.minsocam.org or GeoscienceWorld

221 **Inductively Coupled Plasma Mass Spectrometry (ICP-MS)**

222 An Agilent 7500 Series ICP-MS at Adelaide Microscopy has been used to analyze the Au,
223 Ag and Te contents within the solutions. The concentration levels of the calibration
224 solutions were 500, 200, 100, 50, 20, 10, 5 and 0 ppb (blank) of Au, Ag and Te. Depending
225 on their compositions, solutions were run either unprocessed, or were diluted by factors of
226 100 or 1000 times using 2% HNO_3.

227

228 **Results**

229 **Hydrothermal reactions**

230 X-ray diffraction patterns (Fig. 1) and SEM examinations confirmed that sylvanite has been
231 replaced by other phases via hydrothermal reactions. The products included calaverite, Au-
232 Ag alloy, petzite and hessite (Tables 2 & 4). The morphology of the sylvanite grains is
233 characterized by sharp-edges and smooth surfaces. After the reaction, the product phases
234 (independent of the assemblage) preserved the external dimensions of the primary sylvanite
235 grains; in particular, the edges of the grains remained sharp (Fig. 2a). However, the surfaces
236 of the grains, particularly after 48 hours, became rough with an overgrowth of a porous
237 layer of Au-Ag alloy (Fig. 2b). The surface of the product was always highly porous, with
238 pore sizes up to 1 μm (Figs. 2c; 3a,b). The surface of the grains under the outer highly
239 porous Au-Ag alloy layer was generally a compact but finely porous layer of calaverite
240 (Fig. 2d). The Au-Ag alloy rim was composed of wormlike Au-Ag alloy particles, with
241 diameters ranging from 200 to 1000 nm (Figs. 2b,c; 3a,b). Wire gold also developed locally
242 (up to 5 μm in diameter, 25 μm in length; Fig. 2b). It is clear from cross-sectional SEM

Always consult and cite the final, published document. See http://www.minsocam.org or GeoscienceWorld

243 images that the replacement process initiated at the outer surface of, or along cracks within,
244 the sylvanite crystal fragments (Fig. 3c). Partially replaced grains, particularly when more
245 than 50% of the sylvanite had been converted, contain a mixture of product phases
246 including Au-Ag alloy, 'calaverite', petzite and hessite. While the outside of the grain is
247 always surrounded by a highly porous rim of Au-Ag alloy, the internal textures are
248 complex and somewhat variable, with no clear zoning (Figs. 3c; 4a,b). There are two
249 compositions for calaverite, a porous, Ag-rich-Te-depleted calaverite (hence forth referred
250 to as calaverite-I), and a non-porous calaverite of normal composition (denoted calaverite-II)
251 (e.g., Fig. 4c). The name calaverite, without any qualification, is used for general discussion,
252 where differentiation between the two forms is not important. In general petzite and hessite
253 are closely associated with calaverite: petzite and hessite occur intimately mixed either as
254 small patches or inclusions within calaverite-I (Fig. 4d,f), as veins within calaverite-I
255 (Fig. 4e), or as petzite-hessite lamella next to grains of calaverite-II (Fig. 4c). The
256 calaverite-II generally shares a grain boundary with calaverite-I.

257 Calaverite-I exhibits a similar scale of porosity as Au-Ag alloy with pore diameter of
258 ~1 μm (Figs. 4c,f). In some samples the pores in calaverite are filled with petzite-hessite
259 (Fig. 4f). The petzite-hessite does not appear to be porous. In all cases the grain
260 boundaries/reaction fronts are sharp. Hessite is always fine-grained (≤ 20 μm) and always
261 intergrown with petzite. Orientation analysis by EBSD across the interface between
262 sylvanite and calaverite-I showed that the parent sylvanite exists in a single orientation.
263 However, calaverite provided only poor patterns. In the best example, 8 indexed diffraction
264 patterns over a 10 x 20 μm calaverite-I lamella within sylvanite revealed that calaverite-I

Always consult and cite the final, published document. See http://www.minsocam.org or GeoscienceWorld

265 was polycrystalline (3 orientations); no simple crystallographic relationship between
266 calaverite-I and sylvanite was found in this example.

267 The results of solution ICP-MS (for experiment Series A and B in Table 2) show that the
268 concentrations of Au in the solution are very low (< 5 ppb) in all runs where the solutions
269 were analyzed, and that the concentrations of Ag in the solutions are also low, in the range
270 0.025 (A7) to 197 ppb (B4). These are considerably lower, by several orders of magnitude,
271 than the values expected if there was significant loss of Au and Ag to solution during the
272 reaction. For the sample weight and fluid volume used in these experiments, full dissolution
273 of the sylvanite without any precipitation would liberate approximately 410 ppm Te,
274 200 ppm Au and 60 ppm Ag in solution. The Te concentration is of the order of 10 to
275 200 ppm and higher as the extent of the reaction increases up to a maximum of 283 ppm
276 (A28). In some experiments, particularly where an external oxidant was added (B1-B11) or
277 at low pH, TeO_2(s) was found to have precipitated.

278 Electron microprobe analyses gave the following compositions for the product phases:
279 calaverite-I $(Au_{0.90}Ag_{0.29})Te_2$, with the Ag content varying from $Ag_{0.15}$ to $Ag_{0.49}$; calaverite-
280 II $(Au_{0.93}Ag_{0.07})Te_2$; petzite $(Au_{0.92}Ag_{3.15})Te_2$; hessite $(Ag_{1.89}Au_{0.07})Te$ and Au-Ag alloy
281 $(Au_{0.87}Ag_{0.13})$. The compositions of petzite, hessite and calaverite show some variation, but
282 this is probably a reflection of the uncertainties of the analyses of these finely intergrown
283 minerals rather than any systematic variation in composition with solution conditions
284 (Table 4). Electron microprobe analyses along lines across partially replaced grains show
285 no systematic variation in the chemistry of calaverite-I, calaverite-II, petzite and hessite.

Always consult and cite the final, published document. See http://www.minsocam.org or GeoscienceWorld

Controls on hydrothermal reaction mechanism and kinetics

The effects of temperature, pH, and oxidant or reductant on the reaction mechanism and kinetics were probed using series of experiments conducted under a range of conditions (Table 2).

Effects of temperature. The range and proportion of the products depended on temperature and run-time. At 190 ˚C, sylvanite transformed to a Au-Ag alloy and Te(IV)(aq) (runs C1-C4) in the initial stages of the reaction. After about half of the sylvanite had been transformed to Au-Ag alloy (periods longer than 24 h), calaverite, petzite and hessite appeared amongst the products (runs C5-C7). At 160 ˚C, the reaction was more sluggish and calaverite and petzite were amongst the products after 24 h. For reactions at 220 ˚C, when less than approximately 50% of the sylvanite had been transformed, the dominant products revealed by XRD were calaverite and Au-Ag alloy (Fig. 1) (A1, A2, A8, A9, A15, A22). For runs where more than 50% of sylvanite had been replaced, small amounts of petzite, in addition to calaverite and Au-Ag alloy were seen in the XRD traces. SEM examination of these samples also revealed hessite, Ag_2Te, intergrown with petzite, but in amounts below the detection limit of XRD (Fig. 1) (A3-A7, A10-A14, A16-A21; A23-A28).

Effects of solution pH. Experimental runs exploring the effects of solution pH on the replacement reaction were undertaken by using four solutions, all with 0.01 M NaCl, but different pH at fixed temperature (220 ˚C) and solid-to-fluid-ratio (S/F=0.67 g/L). The solutions used were: milli-Q water [$pH_{220\,^{\circ}C}$ = 5.6, A1-A7], two different phosphate buffer solutions ($pH_{220\,^{\circ}C}$= 2.90, A8-A14; and $pH_{220\,^{\circ}C}$= 8.10, A15-A21), and a borate buffer solution ($pH_{220\,^{\circ}C}$= 9.10, A22-A28). Reactions runs were conducted for 2, 4, 6, 12, 24, 48 and 96 hours. The results are summarized in Series A in Table 2 and plotted in Figure 5. After 4 hours, at $pH_{220\,^{\circ}C}$ 9.10, 73% of the sylvanite had been replaced (A23), for $pH_{220\,^{\circ}C}$

Always consult and cite the final, published document. See http://www.minsocam.org or GeoscienceWorld

311 8.10 it is 63% (A16), 32% for $pH_{220\,^{\circ}C}$ 2.10 (A9), and 27% for milli-Q water (A2). Under
312 basic conditions, sylvanite replacement is almost complete after 96 h (A28) and the
313 dominant final product is Au-Ag alloy, but under acidic conditions ($pH_{220\,^{\circ}C}$ 2.10) only ~57%
314 replacement is achieved in this time (A14) and the principal product is calaverite, with
315 minor amounts of petzite + hessite and Au-Ag alloy. Hence, the nature of the products and
316 the extent of the reaction vary with solution pH. Basic pH increases the extent of the
317 reaction, over a given time interval, compared to more acidic conditions. Under basic
318 conditions ($pH_{220\,^{\circ}C}$ 8.10 and 9.10) there is more petzite and hessite in the products (cf. A11
319 to A25), although the relative proportions of the phases appear to have a complex
320 relationship to the solution conditions. For basic pH, the ratio of the calaverite to petzite in
321 the products is approximately 5:1 for runs in which more than 50 mol% sylvanite was
322 replaced. Under more acidic conditions the ratio is closer to 25:1, although the proportion
323 of petzite is relatively small (1 to 3 mol%) and the uncertainties in the QPA are relatively
324 large.

325 **Effects of oxidant or reductant.** The effect of the oxidant [O_2(aq)] availability on the
326 reaction rate was investigated over the pH range examined in this study by adding 20 µl of
327 a 30 wt% H_2O_2 solution (B1-B11, see Table 2). The results from these runs can be
328 compared with data from the hydrothermal experiments in which no additional O_2(aq) was
329 added (A1-A28), and those where reducing conditions were achieved by filling the airspace
330 with a mixture of 1% H_2 in Ar (F1-F4) (see Table 2 and Fig. 5). For the O_2(aq)-rich runs at
331 $pH_{220\,^{\circ}C}$ = 8.10, sylvanite replacement was almost complete after just 4 h (B3) and $TeO_{2(s)}$
332 precipitated. In contrast, without additional O_2(aq) only 57% replacement was achieved in
333 this period (A16) with no $TeO_{2(s)}$ formed. At $pH_{220\,^{\circ}C}$ = 2.90, sylvanite replacement was
334 almost complete within 24 h, compared to ~58% without additional O_2(aq) (A12). At
335 $pH_{220\,^{\circ}C}$ = 9.10 (B11), complete transformation to Au-Ag alloy occurred in 24 h with no
336 tellurides or $TeO_{2(s)}$ present. Under reducing conditions, the reaction was rather sluggish
337 under acidic to neutral conditions but proceeded at $pH_{220\,^{\circ}C}$ = 9.10: after 24 h, 61% of the

Always consult and cite the final, published document. See http://www.minsocam.org or GeoscienceWorld

338 sylvanite had been transformed and the products were 37% calaverite, 5 % petzite and 19%
339 Au-Ag alloy. This can be compared to experiment A26 which has 84% reaction with 56%
340 calaverite, 8% petzite-hessite and 19% Au-Ag alloy and experiment B11, where O_2(aq) has
341 been added and full transformation to Au-Ag alloy was achieved.

342 **Solid-state reactions**

343 In order to compare the results of the hydrothermal reactions with the solid-state reactions,
344 solid-state decomposition experiments were carried out at 220 ˚C in both unsealed and
345 sealed quartz glass tubes. Results are summarized in Table 3. XRD patterns of the heated
346 samples show no change in the sylvanite crystal fragments. At the resolution of SEM
347 images, grain cross-sections images are homogeneous without any phase separation or
348 cracks. This clearly indicates that, at 220 ˚C, the solid-state transformation of sylvanite to
349 Au alloy has not occurred or occurred only to a very small extent (less than 1%) compared
350 to hydrothermal conditions. Whether the sample was heated in air or under vacuum did not
351 affect the progress of any solid-state reaction in dry conditions.

352

353 **Discussion**

354 **Dissolution-reprecipitation versus solid-state diffusion**

355 Sylvanite can be replaced by a range of products, principally Au-Ag alloy and calaverite-I
356 (Ag-rich-Te-depleted calaverite) under hydrothermal conditions. However, no reaction is
357 observed when the samples are heated at the same temperature in the absence of a fluid,
358 which is convincing evidence that this transformation is primarily a fluid-mediated process.
359 Changes in solution chemistry show that the majority of the Te is eventually lost to solution

Always consult and cite the final, published document. See http://www.minsocam.org or GeoscienceWorld

over the course of the reaction, with some precipitation of TeO_2(s) away from the site of the reaction for runs under oxidizing conditions. The extent of TeO_2(s) precipitation depends on the solution pH, with the Te(IV) complexes having lower solubility under acidic conditions. The Au and Ag contents of the solution remain at very low levels (<< 1 ppm), consistent with their low solubility in these solutions and indicative of rapid precipitation during the reaction and a dissolution-reprecipitation mechanism.

The textural features of some of the products (high porosity, microcracking, sharp reaction fronts without a significant gap between the parent and product phases); the dependence of reaction rate and product assemblage on solution chemistry; and the pseudomorphic morphological preservation are all consistent with an interface-coupled dissolution – reprecipitation reaction mechanism (e.g., Putnis and Mezger 2004; Pöml et al. 2007; Niedermeier et al. 2009; Xia et al. 2009; Brugger et al. 2010). Pseudomorphic reactions proceed via coupled dissolution re-precipitation mechanism, where the dissolution of the parent phase is coupled to the precipitation of the product phase at the reaction front, and the reaction rate is controlled by the relative solubilities of the parent and product phases (Putnis 2009). The external dimension of the parent material can only be preserved when the dissolution and precipitation steps are coupled and there is immediate precipitation of the products at the dissolution front. The final product Au-Ag alloy is porous and similar to that formed from the replacement of calaverite by gold under similar hydrothermal conditions (Zhao et al. 2009). The fact that two compositionally distinct calaverites are formed as intermediate products of the transformation of sylvanite to Au-Ag alloy for the reaction at 220 ˚C indicates that the transformation mechanism is multistep and complex. Two competing transformations occur: sylvanite to Au-Ag alloy and sylvanite to calaverite-

Always consult and cite the final, published document. See http://www.minsocam.org or GeoscienceWorld

I (Fig. 6). It is important to note that the sylvanite to calaverite-I reaction only occurs after part of the parent sylvanite has been transformed to Au-Ag alloy, indicating that this reaction is controlled by the amount of Te and Ag in solution. Calaverite-I exhibits porosity and a sharp reaction front with sylvanite, textural features consistent with a dissolution-reprecipitation reaction. The low levels of Ag, but significant Te in solution, are consistent with this hypothesis. This raises the question of the compositional stability field of calaverite. Bindi et al. (2009) reported crystal structural data for a Ag-rich calaverite [$(Au_{0.68}Ag_{0.33})Te_2$] which has almost an identical composition to the sylvanite used in this study [$(Au_{0.68}Ag_{0.35}Sb_{0.01})Te_2$]. This indicates that the compositional fields of sylvanite and calaverite overlap (Fig. 6). Our experiments indicate that calaverite-I forms as a metastable phase with respect to sylvanite under hydrothermal conditions at temperatures of 160 ˚C and above, but under dry conditions at 220 ˚C this transformation does not occur.

The average composition of calaverite-I is $(Au_{0.78}Ag_{0.22})Te_{1.74}$ (calculated on the basis of Au + Ag =1). The compositional range based on some 90 points is Au 0.63 to 0.90; Ag 0.1 to 0.37; Te 1.50 to 1.90, so the general formula is approximately $(Au_{1-x}Ag_x)Te_{2-y}$, with x and y being in the range 0.1 to 0.4. The average composition of the 'normal' calaverite (calaverite-II) formed by the decomposition of calaverite-I is $(Au_{0.93}Ag_{0.07})Te_2$, with a Au range of 0.91 to 0.95 and a Ag range of 0.04 to 0.11 (average 23 points). The hessite composition is $Ag_{1.89}Au_{0.07}Te$ (range Au 0.04 to 0.15; Ag 1.74 to 2.06) and that of petzite $Ag_{3.14}Au_{0.94}Te_2$ (range Ag 2.68 to 3.45; Au 0.86 to 1.14) (Fig. 6). The compositional ranges of hessite and petzite are most probably largely an artifact of the difficulties in obtaining accurate analyses from fine-grained intergrowths, as there is no systematic variation in composition across a reacted grain.

Always consult and cite the final, published document. See http://www.minsocam.org or GeoscienceWorld

406 Texturally it appears that calaverite-I and -II are distinct. Calaverite-I shows high porosity
407 and pores filled with intergrowths of petzite and hessite, and in contrast calaverite-II shows
408 no porosity. We interpret calaverite-I as a metastable quench product that may exist in a
409 different structure under reaction conditions, but without *in situ* diffraction experiments
410 under hydrothermal conditions the exact nature of this metastable phase cannot be
411 established. The Ag-rich tellurides appear as transformation products where the reaction
412 has progressed to about 50% of the sylvanite transformed at 220 ˚C, and act as a sink for
413 the Ag rather than it being released into solution. Petzite and hessite always occur
414 intergrown, and probably represent the product of breakdown of the low temperature
415 metastable phase *X* noted in Cabri (1965). Cabri (1965) gave composition limits of phase *X*
416 as $Ag_{3+x}Au_{1-x}Te_2$ with $0.1 < x < 0.55$, and noted that it broke down to a mixture of low
417 petzite and low hessite below 120 ˚C.

418 As mentioned above, the porosity in calaverite-I is in some cases filled with a fine
419 intergrowth of petzite and hessite. In some samples, however, a calaverite occurs crosscut
420 with veins and lamellae of petzite-hessite and in these textures the calaverite is not porous
421 (calaverite-II). The precipitation of fine-grained mixtures of calaverite, petzite and hessite
422 was not observed in any sample. All of these features are consistent with a set of sequential
423 reactions (Fig. 7): 1) sylvanite is transformed to calaverite-I via a dissolution-
424 reprecipitation reaction; 2) calaverite-I then breaks down via exsolution to calaverite-II plus
425 phase *X* ($Ag_{3+x}Au_{1-x}Te_2$, $0.1 < x < 0.55$). Phase *X* in turn breaks down to a fine
426 intergrowth of petzite and hessite; this later step probably occurs during the quenching of
427 the autoclaves from the reaction temperature (160 to 220 ˚C) to room temperature; 3) both

Always consult and cite the final, published document. See http://www.minsocam.org or GeoscienceWorld

the calaverite-II and phase *X* are subsequently transform to a Au-Ag alloy via coupled dissolution-reprecipitation reactions.

Fluid-mediated pseudomorphic reactions are continuous transformations and their progress depends on open pathways for the transport of fluid and solutes to and from the reaction interface between the parent phase and the product (Putnis and Putnis 2007). Hence porosity is essential to sustain this reaction, by allowing mass transfer (e.g., influx of oxidant and removal of dissolved tellurium for the reactions studied here). The lack of porosity in the calaverite-II-petzite-hessite assemblage indicates that it is the product of a solid-state reaction. Phase relations in the petzite-hessite region of the Au-Ag-Te system are consistent with high metal ion mobility in these phases. Cabri (1965) observed the breakdown of phase *X* to low petzite and low hessite at temperatures as low as 50 ˚C or during grinding under dry conditions. Both petzite and hessite undergo phase transitions from low to intermediate forms at temperatures between 150 and 200 ˚C and both minerals decomposed around 350 to 400 ˚C.

Chemical reactions in the replacement process

At 220 ˚C, the transformation of sylvanite to Au-Ag alloy passes through a number of intermediate phases in the sequence sylvanite → Ag-rich-Te-depleted calaverite (calaverite-I) + Te in solution → calaverite (calaverite-II) + phase *X* → Au-Ag alloy (Fig. 7).

The first step

sylvanite → calaverite-I + Te(aq) Step (1)

Always consult and cite the final, published document. See http://www.minsocam.org or GeoscienceWorld

is an ICDR reaction, but the second step

calaverite-I → calaverite-II + phase *X* Step (2)

is a diffusion-driven solid-state reaction. The final step

calaverite-II + phase *X* → Au-Ag-alloy + Te(aq) Step (3)

is a CDR reaction with loose interface coupling. In addition during quenching of the autoclaves, phase *X* becomes unstable, and breaks down following a diffusion-driven solid-state reaction (exsolution):

phase *X* → petzite + hessite Step (4)

All the dissolution and precipitation reactions depend upon the solution chemistry. The dependence is complex, depending on factors such as pH, availability of oxidants/reductants, and concentrations and speciation of Ag, Au, and Te in solution. The composition of the bulk solution is changing throughout the reaction, and strong compositional gradients may develop near reaction fronts and through porous media, making it challenging to quantify the effect of solution composition on particular reactions. However, a number of general trends in the observed reaction extent data can be related to solution composition and mineral solubility. Mineral solubility in hydrothermal systems is often discussed on the basis of activity-activity diagrams (e.g, O_2(g) vs. pH). However, such two-dimensional diagrams can be difficult to interpret when applied to systems with more than two independent parameters, such as the Au-Te-Ag system of interest here (pH, log $f\,O_2$(g), and activities of the predominant Au, Te and Ag complexes). Diagrams are usually drawn at fixed activities for aqueous components; for components with changing

Always consult and cite the final, published document. See http://www.minsocam.org or GeoscienceWorld

solubilities, this assumption can make the diagrams difficult to interpret. These difficulties are illustrated by previously published diagrams for the Au-Ag-Te system (Zhang and Spry 1994). For example, these diagrams show only one predominant mineral in the mineral stability field, corresponding to the metal-richest phase of interest; however, the phase rule indicates that three minerals should coexist; this number can be lower if mass balance is taken into account. In order to provide simple diagrams to discuss the relative solubilities of Au, Ag and Te as a function of the two main chemical variables (pH and availability of oxidant or reductant), we built diagrams showing the mineral assemblages and the chemistry of the coexisting solution based on full speciation calculations for each point (e.g., Brugger et al. 2003; Kinniburgh and Cooper 2004). The modeled solution contained 0.01 molal chloride and amounts of Au, Ag and Te consistent with the total amounts added (as sylvanite) in our experiments (4 mmolal Te; 1.3 mmolal Au; 0.7 mmolal Ag). Solution pH in the calculations was adjusted by varying the Na concentration in each calculation. The speciation calculations were conducted with the Geochemist's Workbench software (Bethke 2008), and results analyzed using the Matlab programming environment. The diagrams presented in Figure 8 are based on 10,166 individual distributions of species calculations. The thermodynamic properties for the Te species were taken from the review of McPhail (1995); for Au from the review by Usher (2009); and for Ag from Shock (1997) and Sverjensky (1997). For minerals, properties for calaverite, tellurite and tellurium are taken from McPhail (1995); native gold and silver from Helgeson (1978); and hessite and petzite from Echmaeva and Osadchii (2009). Using the petzite properties of Echmaeva and Osadchii (2009), petzite was always undersaturated relative to other Ag-Au minerals (Figs. 8d, e). To illustrate mineral assemblages expected if petzite would be more stable

Always consult and cite the final, published document. See http://www.minsocam.org or GeoscienceWorld

494 than expected (e.g., kinetically favored by nucleation), we also performed calculations with
495 increased stability of petzite ($\Delta G_f^{200°C}$ = -79.66 kJ/mole according to Echmaeva and
496 Osadchii (2009); -132.94 kJ/mole used in the calculations of Figure 8f).

497 The calculations show that at 200 ˚C, aqueous Te concentrations in excess of 1 ppm can be
498 achieved either under oxidizing conditions ($\log fO_2(g) > -30$) or under reducing conditions
499 at high pH ($pH_{200\ °C} > 9$). This is consistent with the observation that under reducing
500 conditions, the reaction did not proceed under near-neutral conditions (F1, Table 2), with
501 very little reaction at $pH_{220\ °C}$ 2.90 (F2), slightly more at $pH_{220\ °C}$ 8.10 (F3), and extensive
502 reaction at $pH_{220°C}$ 9.10 (F4).

503

504 **Dissolution of sylvanite.** Taking into account the dominant aqueous species in the system,
505 the dissolution of sylvanite in the presence of O_2(aq) can be written depending on pH, as:

506 Acidic conditions (buffer P2, $pH_{220\ °C}$ = 2.90; Fig. 8):

507 $$Au_xAg_{2-x}Te_4(s) + 4.5\ O_2(aq) + 2\ Cl^- + 2H^+ + 3H_2O$$

508 $$= xAuCl(aq) + (2\text{-}x)AgCl(aq) + 4H_2TeO_3(aq); \qquad (1)$$

509 basic conditions (buffers P7, $pH_{220\ °C}$ = 8.10 and B10, $pH_{220\ °C}$ = 9.10):

510 $$Au_xAg_{2-x}Te_4(s) + 4.5\ O_2(aq) + (2 - x)\ Cl^- + (2 + 2x)\ OH^- + H_2O$$

511 $$= xAu(OH)_2^- + (2 - x)AgCl(aq) + 4HTeO_3^-. \qquad (2)$$

512 Under oxidizing conditions, the oxidation of Te to Te^{4+} is necessary to allow Te to be
513 removed into solution. The oxidation of Te is confirmed by the presence TeO_2(s)

Always consult and cite the final, published document. See http://www.minsocam.org or GeoscienceWorld

514 precipitates that were detected at all studied pHs, and by the fact that when concentrated
515 HCl was added to the reacted solutions they turn bright yellow, a coloration due to the
516 formation of Te(IV) chlorocomplexes (Nabivanets and Kapantsyan 1968). Hence, sylvanite
517 dissolution is an oxidation process, and the concentration of oxygen plays an important role
518 in controlling the dissolution rate. The presence of dissolved oxygen in the fluid at the
519 reaction interface is critical for the reaction to proceed. Thus the addition of O_2(aq)
520 increased the reaction rate.

521 Under reducing [H_2(g) present] and highly basic conditions (buffer B10, $pH_{220°C}$ =9.10), the
522 dissolution of sylvanite can be written as (Fig. 8):

523 $$Au_xAg_{2-x}Te_4(s) + (2-x)\ Cl^- + (2 + 2x)\ OH^- + H_2(g)$$

524 $$= xAu(OH)_2^- + (2 - x)AgCl(aq) + 2Te_2^{2-} + 2H_2O. \quad (3)$$

525 In this case, the dissolution is a reduction because Te is lost into solution as a polytelluride
526 complex (Te_2^{2-}). Hence, increased availability of H_2(g) in the system is expected to increase
527 reaction rates.

528 **Precipitation of calaverite-I.** Calaverite-I is likely to form via precipitation from aqueous
529 solution, according to the reaction (oxidizing, acidic to slightly basic conditions):

530 $$(1 - x)\ AuCl(aq) + x\ AgCl(aq) + (2 - x)\ H_2TeO_3(aq)$$

531 $$= (Au_{1-x}Ag_x)Te_{2-y} + Cl^- + H^+ + (1.5 - x)\ H_2O + (2.25 - x)\ O_2(aq) \quad (4)$$

532 Reaction 4 describes the reduction of Au(I) and Te(IV), controlled by the activities of
533 O_2(aq) and that of the predominant Au, Ag and Te complexes. Ag plays an important role
534 as it is not lost to the bulk of the solution. The decrease of oxygen activity favors the

Always consult and cite the final, published document. See http://www.minsocam.org or GeoscienceWorld

precipitation of calaverite-I. Oxygen is continuously removed by the oxidation of Te, and the oxidation product leaves the reaction front by mass transport in the fluid due to its high solubility. Calaverite-I precipitation occurred under all the studied conditions. That is mainly because of the dissolution of sylvanite, which contains 67 at% Te, produces high concentrations of Te at the reaction front. Homogeneous nucleation of metastable calaverite-I appears to be facilitated by the sylvanite surface, although no epitaxial relationship has been observed so far. The nucleation of calaverite-I appears to be followed by the growth of the calaverite nuclei. As soon as a thin calaverite-I rim forms, the phase can easily grow onto this substrate. This dissolution-reprecipitation process continues until all of the sylvanite has dissolved and most of the calaverite-I has precipitated.

Phase X. Phase *X* is likely to form via a solid-state reaction due to the breakdown of the metastable Ag-rich-Te-depleted calaverite-I in favor of an assemblage of near-stoichiometric calaverite-II plus phase *X*, according to the reaction:

$$(Au_{1-x}Ag_x)Te_{2-y} \rightarrow a\ AuTe_2 + b\ Ag_{3+z}Au_{1-z}Te_2, \quad (5)$$

Reaction 5 is controlled by solid-state diffusion and to a certain extent by the solution chemistry as at low pH little petzite forms. This may reflect a variation in the composition of the calaverite-I with solution composition.

Transformation of calaverite-I to Au-Ag alloy. The transformation of the calaverite-I (or its solid-state decomposition products) to Au-Ag alloy is also a dissolution-reprecipitation reaction. The Au-Ag alloy is likely to form via precipitation from aqueous solution, according to the reaction (acidic, oxidizing conditions):

$$x\ AuCl(aq) + (1 - x)\ AgCl(aq) + 0.5\ H_2O$$

$$= Au_xAg_{(1-x)} + Cl^- + H^+ + 0.25\ O_2(aq)\ (x \leq 1) \quad (6)$$

Always consult and cite the final, published document. See http://www.minsocam.org or GeoscienceWorld

Reaction 6 describes the reduction of Au(I) and Ag(I), controlled by the redox potential of the fluid at the reaction front. The decrease of oxygen activity favors the precipitation of Au-Ag alloy. Oxygen is continuously removed by the oxidation of Te, and the oxidation product leaves the reaction front by mass transport in the fluid due to its higher solubility. The dissolution of sylvanite causes the concentration of aqueous Au and Ag complexes at the reaction front to increase. After a period of time, the concentration of Au and Ag will become supersaturated and nucleation of Au-Ag alloy will occur. As the Te concentrations built up in the fluid, Au-Ag alloy precipitation will compete with the precipitation of Ag-rich calaverite.

The overall replacement reaction of calaverite by native gold can be written as:

$$AuTe_2(s) + 2\ O_2(aq) + 2\ H_2O = Au(s) + 2\ H_2TeO_3(aq). \quad (7)$$

Dissolution of calaverite under acidic to slightly basic ($pH_{220\ ^\circ C}$ 2–7.5):

$$AuTe_2(s) + 2.5\ H_2O + 2.25\ O_2(aq) = 2\ H_2TeO_3(aq) + AuOH(aq). \quad (8)$$

And precipitation of gold:

$$AuOH(aq) = Au(s) + 0.5H_2O + 0.25O_2(aq). \quad (9)$$

A previous study on the transformation of calaverite showed that calaverite will be replaced by porous gold under all studied conditions via a coupled dissolution reprecipitation process (Zhao et al. 2009, 2010). However, compared with the reaction extent in these studies, the reaction rate of the transformation from calaverite to Au-Ag alloy is lower. At $pH_{220\ ^\circ C}$=9.10, only 19% of gold plus 56% of calaverite-I are formed after 24 hours reaction, while Zhao et al. (2009) observed almost complete transformation of calaverite to gold in

Always consult and cite the final, published document. See http://www.minsocam.org or GeoscienceWorld

579 the same period under similar solution conditions. The difference in reaction rates between
580 the transformation starting with sylvanite or starting with pure calaverite points both to the
581 effects of Ag in the system and possibly the effects of the Te-depleted stoichiometry of
582 calaverite-I.

583

584 **Applications and implications for reactions under hydrothermal conditions**

585 The nature of the sylvanite transformation has implications for the treatment of telluride
586 gold ores and for understanding the origin of some unusual telluride assemblages in Nature.
587 At 220 ˚C, solid-state replacement of sylvanite by gold is slow (months), but sylvanite
588 grains ~100 μm in size can be fully replaced in 96 hours under hydrothermal conditions,
589 providing a possible low-emission and lower energy alternative to roasting as a pre-
590 treatment of telluride-rich gold ores (Spry et al. 2004; Zhao et al. 2010).

591 In this paper we are primarily concerned with the nature of the mechanism of the
592 transformation and the interplay between solution-driven dissolution-reprecipitation
593 reactions and solid-state reactions. The experimental textures obtained in this study are
594 remarkably complex (e.g., Fig. 4). Some of the texture may be easily misinterpreted; for
595 example the vein-like textures of Figures 4a,e may be related to some deformation rather
596 than exsolution, or the complex textures may be interpreted in terms of complex fluid or
597 P,T path evolution at deposit scale. The textural complexity in the replacement of sylvanite
598 in our experiments arises from a complex interaction among solid-state and coupled
599 dissolution-reprecipitation reactions. Such complex patterns are expected to arise in some
600 sulfide systems under mild hydrothermal conditions (e.g, Cu-(Fe)-S, Ag-S systems, where

Always consult and cite the final, published document. See http://www.minsocam.org or GeoscienceWorld

601 the solid-state mobility of Cu^{+} and Ag^{+} ions is relatively high at moderate temperatures),
602 but may also affect oxide and silicate systems at higher temperatures.

603

604 **Acknowledgements**

605 We thank Len Green, Aoife McFadden and Angus Netting from Adelaide Microscopy
606 Center for their assistance in using the FESEM, EBSD, ICP-MS and electron microprobe.
607 This work has been made possible by the financial support of the Australian Research
608 Council (grants DP0880884 and DP1095069). We also thank Associate Editor Daniel
609 Harlov, Iain Pitcairn and an anonymous referee for their constructive reviews of the
610 manuscript.

611

612 # Reference

613 Bachmann, F., Hielscher, R., and Schaeben, H. (2010) Texture analysis with MTEX - free
614 and open source software toolbox. Solid State Phenomena, 160, 63-68.

615 Bethke, C.M. (2008) Geochemical and biogeochemical reaction modeling (2^{nd} edition). 564
616 p. Cambridge University Press, New York.

617 Bindi, L., Arakcheeva, A., and Chapuis, G. (2009) The role of silver on the stabilization of
618 the incommensurately modulated structure in calaverite, $AuTe_2$. American
619 Mineralogist, 94, 728-736.

Always consult and cite the final, published document. See http://www.minsocam.org or GeoscienceWorld

Brugger, J., McPhail, D.C., Wallace, M., and Waters, J. (2003) Formation of willemite in hydrothermal environments. Economic Geology, 98, 819-835.

Brugger, J., McFadden, A., Lenehan, C.E., Etschmann, B., Xia, F., Zhao, J., and Pring, A. (2010) A Novel route for the synthesis of mesoporous and low-thermal stability materials by coupled dissolution-reprecipitation reactions: mimicking hydrothermal mineral formation. Chimia, 64, 693-698.

Cabri, L.J. (1965) Phase relations in the Au-Ag-Te systems and their mineralogical significance. Economic Geology, 60, 1569-1606.

Cook, N.J., Ciobanu, C.L., Spry, P.G., and Voudouris, P. (2009) Understanding gold-(silver)-telluride-(selenide) mineral deposits. Episodes, 32, 249-263.

Echmaeva, E.A. and Osadchii, E.G. (2009) Determination of the thermodynamic properties of compounds in the Ag-Au-Se and Ag-Au-Te systems by the EMF method. Geology of Ore Deposits, 51, 247-258.

Helgeson, H.C., Delany, J.M., Nesbitt, H.W., and Bird, D.K. (1978) Summary and critique of the thermodynamic properties of rock-forming minerals. American Journal of Science, 278A, 229.

Howard, C. (1982) The approximation of asymmetric neutron powder diffraction peaks by sums of Gaussians. Journal of Applied Crystallography, 15, 615-620.

Hunter, B.A. (1998) Rietica—A visual Rietveld program. International Union of Crystallography Commission on Powder Diffraction Newsletter, 20, 21-23.

Always consult and cite the final, published document. See http://www.minsocam.org or GeoscienceWorld

Kinniburgh, D.G. and Cooper, D.M. (2004) Predominance and mineral stability diagrams revisited. Environmental Science & Technology, 38, 3641-3648.

McPhail, D.C. (1995) Thermodynamic properties of aqueous tellurium species between 25 and 350 ˚C. Geochimica et Cosmochimica Acta, 59, 851-866.

Nabivanets, B.I. and Kapantsyan, E.E. (1968) The tellurium(IV) state in HCl and LiCl solutions. Russian Journal of Inorganic Chemistry, 13, 946–949.

Niedermeier, D., Putnis, A., Geisler, T., Golla-Schindler, U., and Putnis, C. (2009) The mechanism of cation and oxygen isotope exchange in alkali feldspars under hydrothermal conditions. Contributions to Mineralogy and Petrology, 157, 65-76.

Pals, D.W. and Spry, P.G. (2003) Telluride mineralogy of the low-sulfidation epithermal Emperor gold deposit, Vatukoula, Fiji. Mineralogy and Petrology, 79, 285-307.

Pertlik, F. (1984) Kristallchemie natürlicher Telluride. I: Verfeinerung der Kristallstruktur des Sylvanits, $AuAgTe_4$. Tschermaks Mineralogische und Petrographische Mitteilungen, 33, 203-212 (in German).

Pöml, P., Menneken, M., Stephan, T., Niedermeier, D.R.D., Geisler, T., and Putnis, A. (2007) Mechanism of hydrothermal alteration of natural self-irradiated and synthetic crystalline titanate-based pyrochlore. Geochimica et Cosmochimica Acta, 71, 3311-3322.

Putnis, A. (2002) Mineral replacement reactions: from macroscopic observations to microscopic mechanisms. Mineral Magazine, 66, 689-708.

Always consult and cite the final, published document. See http://www.minsocam.org or GeoscienceWorld

Putnis, A. (2009) Mineral Replacement Reactions. Reviews in Mineralogy and Geochemistry, 70, 87-124.

Putnis, A. and Putnis, C.V. (2007) The mechanism of reequilibration of solids in the presence of a fluid phase. Journal of Solid State Chemistry, 180, 1783-1786.

Putnis, C.V. and Mezger, K. (2004) A mechanism of mineral replacement: isotope tracing in the model system KCl-KBr-H_2O. Geochimica et Cosmochimica Acta, 68, 2839-2848.

Reithmayer, K., Steurer, W., Schulz, H., and de Boer, J.L. (1993) High-pressure single-crystal structure study on calaverite, $AuTe_2$. Acta Crystallographica, B49, 6-11.

Rietveld, H. (1969) A profile refinement method for nuclear and magnetic structures. Journal of Applied Crystallography, 2, 65-71.

Qian, G., Brugger, J., Skinner, W.M., Chen, G., and Pring, A. (2010) An experimental study of the mechanism of the replacement of magnetite by pyrite up to 300 ˚C. Geochimica et Cosmochimica Acta, 74, 5610-5630.

Qian, G., Xia, F., Brugger, J., Skinner, W.M., Bei, J., Chen, G., and Pring, A. (2011) Replacement of pyrrhotite by pyrite and marcasite under hydrothermal conditions up to 220 ˚C: An experimental study of reaction textures and mechanisms. American Mineralogist, 96, 1878–1893.

Schutte, W.J. and de Boer, J.L. (1988) Valence fluctuations in the incommensurately modulated structure of calaverite $AuTe_2$. Acta Crystallographica, B44, 486-494.

Always consult and cite the final, published document. See http://www.minsocam.org or GeoscienceWorld

Shackleton, J.M., Spry, P.G., and Bateman, R. (2003) Telluride mineralogy of the golden mile deposit, Kalgoorlie, Western Australia. Canadian Mineralogist, 41, 1503-1524.

Shock, E.L., Sassani, D.C., Willis, M., and Sverjensky, D.A. (1997) Inorganic species in geologic fluids - correlations among standard molal thermodynamic properties of aqueous ions and hydroxide complexes. Geochimica et Cosmochimica Acta, 61, 907-950.

Spry, P.G., Chryssoulis, S., and Ryan, C.G. (2004) Process mineralogy of gold: gold from telluride-bearing ores. Journal of the Minerals, Metals and Materials Society, 56, 60-62.

Strunz, H. and Nickel, E.H. (2001) Strunz mineralogical tables: chemical structural mineral classification system (9th edition), 870 pp. Schweizerbart, Stuttgart.

Sverjensky, D.A., Shock, E.L., and Helgeson, H.C. (1997) Prediction of the thermodynamic properties of aqueous metal complexes to 1000 ˚Cand 5 kb. Geochimica et Cosmochimica Acta, 61, 1359-1412.

Tenailleau, C., Pring, A., Etschmann, B., Brugger, J., Grguric, B., and Putnis, A. (2006) Transformation of pentlandite to violarite under mild hydrothermal conditions. American Mineralogist, 91, 706-709.

Tooth, B., Ciobanu, C., O'Neil, B., Green, L., and Brugger, J. (2011) Bi-melt formation and gold scavenging from hydrothermal fluids: An experimental study. Geochimica Cosmochimica Acta, 75, 5423-5443.

Always consult and cite the final, published document. See http://www.minsocam.org or GeoscienceWorld

Usher, A., McPhail, D.C., and Brugger, J. (2009) A spectrophotometric study of aqueous Au(III) halide-hydroxide complexes at 25-80 ˚C. Geochimica et Cosmochimica Acta, 73, 3359-3380.

Vaughan, D.J. and Craig, J.R. (1978) Mineral chemistry of metal sulfides, Cambridge University Press, Cambridge. 493 pp.

Xia, F., Zhou, J., Pring, A., Ngothai, Y., O'Neill, B., Brugger, J., Chen, G., and Colby, C. (2007) The role of pyrrhotite (Fe_7S_8) and the sample texture in the hydrothermal transformation of pentlandite ($(Fe,Ni)_9S_8$) to violarite ($(Ni,Fe)_3S_4$). Reaction Kinetics and Catalysis Letters, 92, 257-266.

Xia, F., Zhou, J., Brugger, J., Ngothai, Y., O'Neill, B., Chen, G., and Pring, A. (2008) Novel Route To Synthesize Complex Metal Sulfides: Hydrothermal Coupled Dissolution-Reprecipitation Replacement Reactions. Chemistry of Materials, 20, 2809-2817.

Xia, F., Brugger, J., Chen, G., Ngothai, Y., O'Neill, B., Putnis, A., and Pring, A. (2009) Mechanism and kinetics of pseudomorphic mineral replacement reactions: A case study of the replacement of pentlandite by violarite. Geochimica et Cosmochimica Acta, 73, 1945-1969.

Zhang, X.M. and Spry, P.G. (1994) Calculated Stability of Aqueous Tellurium Species Calaverite, and Hessitc at Elevated Temperatures. Economic Geology and the Bulletin of the Society of Economic Geologists, 89, 1152-1166.

Always consult and cite the final, published document. See http://www.minsocam.org or GeoscienceWorld

720 Zhao, J., Brugger, J., Grundler, P.V., Xia, F., Chen, G., and Pring, A. (2009) Mechanism
721 and kinetics of a mineral transformation under hydrothermal conditions: Calaverite
722 to metallic gold. American Mineralogist, 94, 1541-1555.

723 Zhao, J., Xia, F., Pring, A., Brugger, J., Grundler, P.V., and Chen, G. (2010) A novel pre-
724 treatment of calaverite by hydrothermal mineral replacement reactions. Minerals
725 Engineering, 23, 451-453.

Always consult and cite the final, published document. See http://www.minsocam.org or GeoscienceWorld

726

727 **TABLE 1. Composition of buffer solutions**

pH		Buffer	Components		
meas.*	calc.#	ID			
2.10	2.90	P2	0.1044*M* H_3PO_4	0.0954*M* NaH_2PO_4	0.01*M* NaCl
6.90	8.10	P7	0.0680*M* NaH_2PO_4	0.1310*M* Na_2HPO_4	0.01*M* NaCl
9.80	9.10	B10	0.1064*M* H_3BO_3	0.0936*M* NaOH	0.01*M* NaCl

*pH values were measured at room temperature (~25 ˚C).

#pH at reaction temperature (220 ˚C) were calculated using Geochemist's Work Bench (GWB) based on the nominal compositions.

728

729

730

731 **TABLE 2. Summary of the hydrothermal reactions conditions and results**[*]

Run No.	T/(˚C)	Reaction Solution[#]	Time (h)	Products and molar percentage (mol%)[§]	Concentrations of Au, Ag and Te[‡]		
					Au (ppb)	Ag (ppb)	Te (ppm)
A1	220	W	2	Sy(84)Ca(13)AA(2)	0.09	0.18	10.8
A2	220	W	4	Sy(73)Ca(18)AA(9)	1.64	4.16	27.5
A3	220	W	6	Sy(46)Ca(41)Pe(1)AA(12)	5.36	19.26	4.7
A4	220	W	12	Sy(41)Ca(50)Pe(3)AA(6)	0.69	5.25	9.8
A5	220	W	24	Sy(45)Ca(51)Pe(2)AA(3)	0.11	1.41	7.6
A6	220	W	48	Sy(34)Ca(56)Pe(2)AA(8)	<0.04	0.78	3.5
A7	220	W	96	Sy(39)Ca(56)Pe(3)AA(3)	<0.04	<0.07	1.8
A8	220	P2	2	Sy(84)Ca(14)AA(3)	0.14	44.70	8.5
A9	220	P2	4	Sy(68)Ca(26)AA(6)	0.61	14.13	37.8
A10	220	P2	6	Sy(49)Ca(44)Pe(1)AA(6)	0.46	33.96	28.6
A11	220	P2	12	Sy(38)Ca(57)Pe(3)AA(3)	0.14	0.67	36.2
A12	220	P2	24	Sy(42)Ca(54)Pe(2)AA(3)	0.06	38.43	32.6
A13	220	P2	48	Sy(40)Ca(54)Pe(1)AA(4)	<0.04	4.90	47.4
A14	220	P2	96	Sy(43)Ca(54)Pe(2)AA(1)	<0.04	0.44	32.6
A15	220	P7	2	Sy(81)Ca(6)AA(13)	0.21	4.12	27.6
A16	220	P7	4	Sy(37)Ca(41)Pe(4)AA(17)	0.09	14.10	99.6
A17	220	P7	6	Sy(20)Ca(45)Pe(7)AA(27)	0.06	92.67	50.7
A18	220	P7	12	Sy (12)Ca(50)Pe(8)AA(29)	<0.04	73.08	27.2
A19	220	P7	24	Sy(18)Ca(61)Pe(7)AA(15)	<0.04	21.54	80.2
A20	220	P7	48	Sy(20)Ca(65)Pe(6)AA(9)	<0.04	0.61	31.5
A21	220	P7	96	Sy(5)Ca(75)Pe(10)AA(11)	<0.04	1.38	28.8
A22	220	B10	2	Sy(78)Ca(12)AA(10)	0.16	5.99	37.6
A23	220	B10	4	Sy(27)Ca(37)Pe(7)AA(29)	0.30	1.78	274.8
A24	220	B10	6	Sy(18)Ca(40)Pe(11)AA(32)	0.17	13.20	253.2
A25	220	B10	12	Sy(17)Ca(49)Pe(9)AA(25)	0.09	5.31	216.9
A26	220	B10	24	Sy(16)Ca(56)Pe(8)AA(19)	0.08	31.35	205.9
A27	220	B10	48	Sy(13)Ca(50)Pe(8)AA(29)	0.09	46.36	233.7
A28	220	B10	96	Sy(3)Ca(25)Pe(10)AA(62)	<0.04	0.17	283.2
B1[†]	220	P7	1	Sy(64)Ca(24)Pe(1)AA(11)	<0.04	50.31	128.6
B2[†]	220	P7	2	Sy(39)Ca(22)Pe(3)AA(36)	<0.04	132.30	235.6
B3[†]	220	P7	4	Sy(2)Ca(3)Pe(3)AA(92)	<0.04	112.10	213.3
B4[†]	220	P7	6	AA(100)	0.29	197.10	221.8
B5[†]	220	P7	12	AA(100)	--	--	--
B6[†]	220	P2	2	Sy(10)Ca(3)Pe(2)AA(21)Te(64)	--	--	--
B7[†]	220	P2	4	Sy(1) AA(29)Te(70)	--	--	--
B8[†]	220	P2	6	AA(35)Te(65)	--	--	--
B9[†]	220	P2	24	AA(53)Te(47)	--	--	--
B10[†]	220	W	24	AA(31)Te (69)	--	--	--
B11[†]	220	B10	24	AA(100)	--	--	--
	190	W	24	Sy(89)AA(11)			

C1					--	--	--
C2	190	P2	24	Sy(89)AA(11)	--	--	--
C3	190	P7	24	Sy(70)AA(30)	--	--	--
C4	190	B10	24	Sy(55)AA(45)	--	--	--
C5	190	B10	48	Sy(37)Pe(5) AA(58)	--	--	--
C6	190	B10	96	Sy(26)Ca(31)Pe(4)AA(38)	--	--	--
C7	190	B10	144	Sy(11)Ca(29)Pe(8)AA(53)	--	--	--
D1	160	B10	24	Sy(69)Ca(16)Pe(4)AA(11)	--	--	--
D2	160	B10	48	Sy(44)Ca(15)Pe(10)AA(31)	--	--	--
D3	160	B10	96	Sy(34)Ca(21)Pe(11)AA(34)	--	--	--
D4	160	B10	144	Sy(14)Ca(11)Pe(13)AA(62)	--	--	--
F1‖	220	W	24	Sy (100)	--	--	--
F2‖	220	P2	24	Sy(97)AA(3)	--	--	--
F3‖	220	P7	24	Sy(89)AA(11)	--	--	--
F4‖	220	B10	24	Sy(39)Ca(37)Pe(5)AA(19)	--	--	--

* The ratio between the weight of sylvanite and the volume of fluid is 0.67.

"W" Milli-Q water, "P" phosphate buffer solution, "B" borate buffer solution. For respective compositions refer to Table 1.

§ Obtained from XRD patterns by Rietveld quantitative phase analysis. "Sy" stands for sylvanite ($AuAgTe_4$) phase, "Ca" calaverite ($AuTe_2$), "AA" Gold and Silver alloy, "Pe" Petzite ($A_{g3}AuTe_2$), and "Te" for tellurium dioxide (TeO_2). Error on the phase proportion is estimated to 5% on each determination.

‡ Obtained from ICP-MS by the analysis of Au, Ag and Te concentrations in the reacted solution samples. The detection limit for Au, Ag and Te are 0.04 ppb, 0.07 ppb and 0.2 ppm, respectively. The concentration would be Au (57-67 ppm), Ag (187-217 ppm) and Te (385-446 ppm), if the 10 mg (±0.5) of sylvanite is all dissolved in the solution.

† 30wt% H_2O_2 solution was added into the buffer solutions (No. B1-B11).

|| Reactions (No. F1-F4) were filled with Ar mixture containing 1% H_2 before sealing.

732

733

TABLE 3. The solid-state transformation experiments by heating sylvanite grains at 220 ℃in both unsealed and sealed evacuated quartz glass tubes

Run No.	T/(˚C)	Time/(days)	Air conditions	Results
G1	220	1	Air	No reaction
G2	220	2	Air	No reaction
G3	220	56	Air	No reaction
H1	220	1	Vacuum	No reaction
H2	220	2	Vacuum	No reaction
H3	220	56	Vacuum	No reaction

TABLE 4. Compositions of the original sylvanite and product phases

Mineral Name	n	Au (wt%)	Ag (wt%)	Te (wt%)	Composition
Sylvanite	12	31.2(31.0-31.5)	8.9(8.7-9.1)	60.3(60.1-60.9)	$Au_{1.34}Ag_{0.70}Te_4$
Calaverite I	54	39.5(33.2-41.6)	5.3(2.6-18.3)	56.1(50.0-57.3)	$Au_{0.81}Ag_{0.19}Te_{1.77}$
Calaverite II	23	41.4(40.7-42.2)	1.8(1.1-2.8)	57.5(56.6-58.2)	$Au_{0.93}Ag_{0.07}Te_2$
Petzite	13	22.6(14.7-25.7)	45.1(42.2-50.9)	33.6(31.2-35.7)	$Au_{0.88}Ag_{3.18}Te_2$
Hessite	13	8.1(5.0-11.0)	53.2(52.2-57.7)	37.0(36.0-39.0)	$Au_{0.14}Ag_{1.77}Te$
Au-Ag alloy	5	93.6(94.7-92.1)	7.3(7.6-7.0)	--	$Au_{0.87}Ag_{0.13}$

Figure captions

Figure 1. Powder x-ray diffraction traces illustrating the progress of the hydrothermal reaction of sylvanite and the range of products formed including Au-Ag alloy, petzite, and calaverite. Elemental Si was used as an internal phase standard.

Figure 2. Secondary electron images showing reaction textures from hydrothermal reactions. **(a)** Sharp edges of a reacted grain, showing the preservation of the external dimensions of the primary sylvanite grains (run A26). **(b,c,d)** 48 hour reacted grain from run A27. **(b)** Grain showing an overgrowth of a porous Au-Ag alloy layer. Note wire–shaped Au-Ag alloy crystals up to 20 μm in length. **(c)** Close up view showing the porosity within the Au-Ag alloy. **(d)** Surface of the grain under the outer shell of porous Au-Ag alloy, consisting of generally compact but finely porous calaverite-I.

Figure 3. Imaging of partially replaced grains from run A28. (**a,b**) Secondary electron images showing the surface **(a)** and the cross section **(b)** of the Au-Ag alloy rim. **(c)** Back-scattered electron images of cross section of a partially reacted grain.

Figure 4. Back-scattered electron and EMP elemental images of cross-section of partially reacted grains illustrating the range of products and textures of the calaverite-I, calaverite-II, petzite, hessite, and Au-Ag alloy (different grains from run A25). **(a)** Overview of a grain. (**b**) Qualitative elemental map of the grain shown in (**a**), obtained using the EMP; red: Au; green: Ag; blue: Te; horizontal resolution ~1 μm. (**c**) Boundary between calaverite-I and calaverite-II, marked by petzite+hessite lamellae. **(d)** Petzite-hessite lamella next to a calaverite-I grain. **(e)** Vein of petzite-hessite in calaverite-I (area shown in (**a**)). **(f)** Petzite and hessite occurring intimately mixed either as small patches or inclusions within calaverite-I.

Figure 5. Plots of reaction extent versus reaction time at different pH and oxidation conditions. Plots A and B represent experiments B6 to B9 and B1 to B5 respectively. Plots C to F represent experiments A1 to A7; A8 to A14; A15 to A21 and A22 to A28 respectively (see Table 2) . To take into account the errors from both sample preparation and Rietveld fit, the error on the phase proportion is estimated to 5% on each determination.

Figure 6. The Au-Ag-Te ternary diagram, showing the composition of sylvanite and other product phases.

Figure 7. Overview of the proposed reaction paths of the hydrothermal reaction of sylvanite.

Figure 8. Numerical simulation of mineral solubility and aqueous speciation in Au-Ag-Te solutions at 200 °C. **(a)** Gold solubility and predominant aqueous complex. **(b)** Tellurium solubility and predominant aqueous complex. **(c)** Silver solubility and predominant aqueous complex. **(d)** Saturation index [log(Q/K)] for the mineral petzite. **(e)** Mineral assemblages. **(f)** Mineral assemblages obtained by increasing the stability of petzite relative to the properties provided by Echmaeva and Osadchii (2009) (see text for details).

.

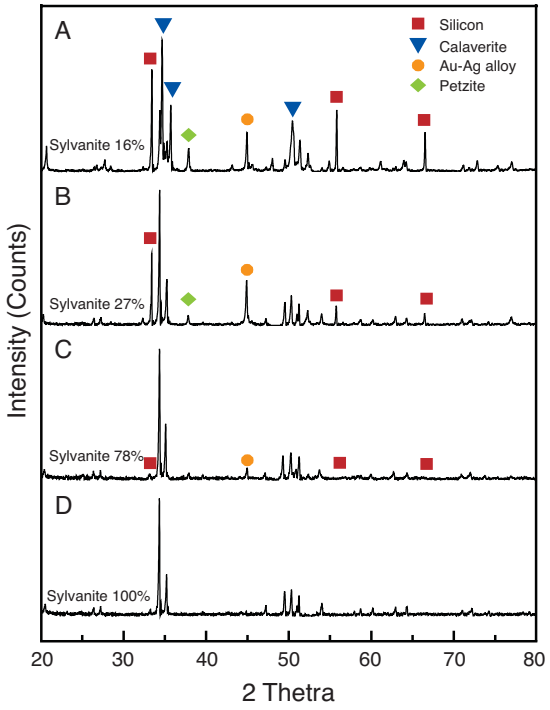
A
B
C
D
Silicon
Calaverite
Au-Ag alloy
Petzite
Sylvanite 16%
Sylvanite 27%
Sylvanite 78%
Sylvanite 100%
Intensity (Counts)
20
30
40
50
60
70
80
2 Thetra

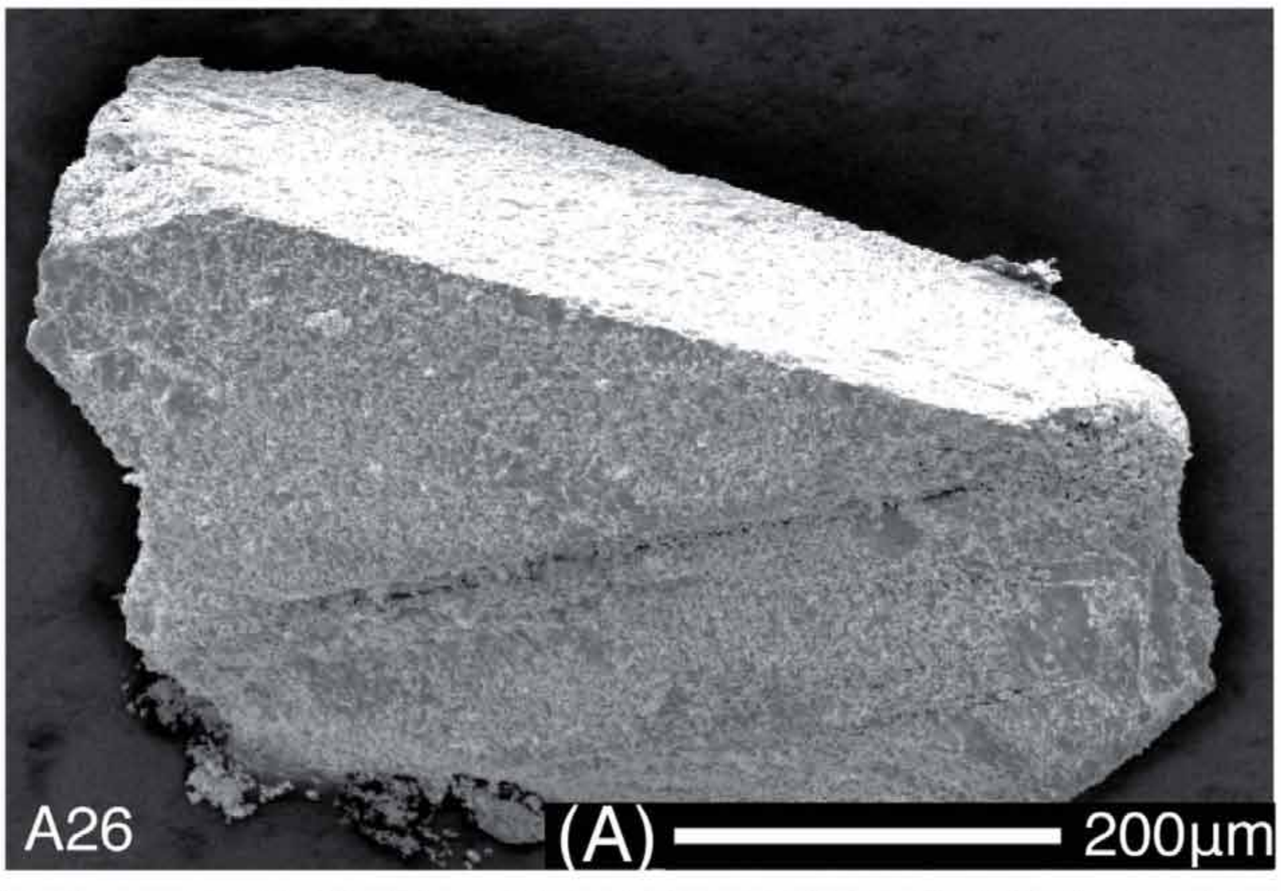
A26
(A)
200µm

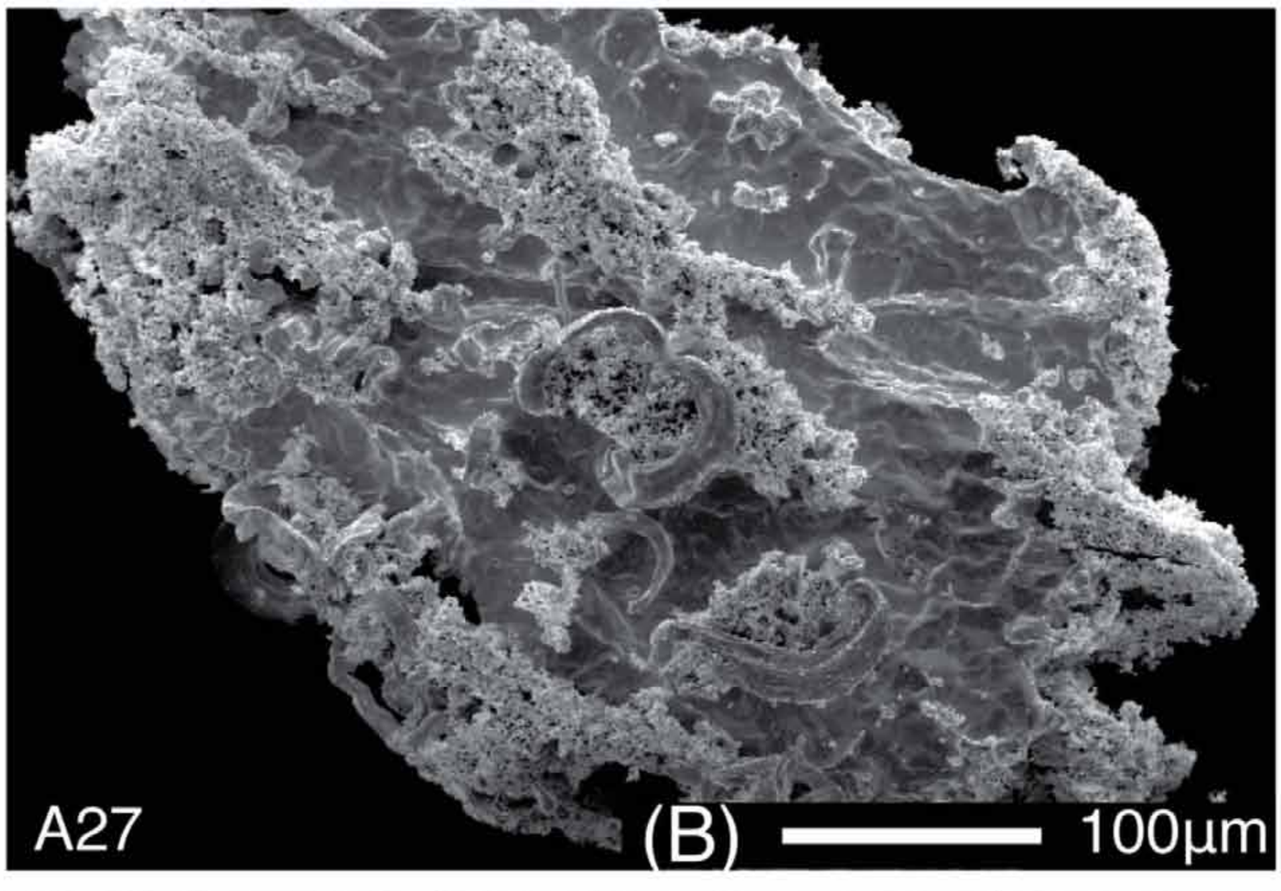
A27
(B)
100µm

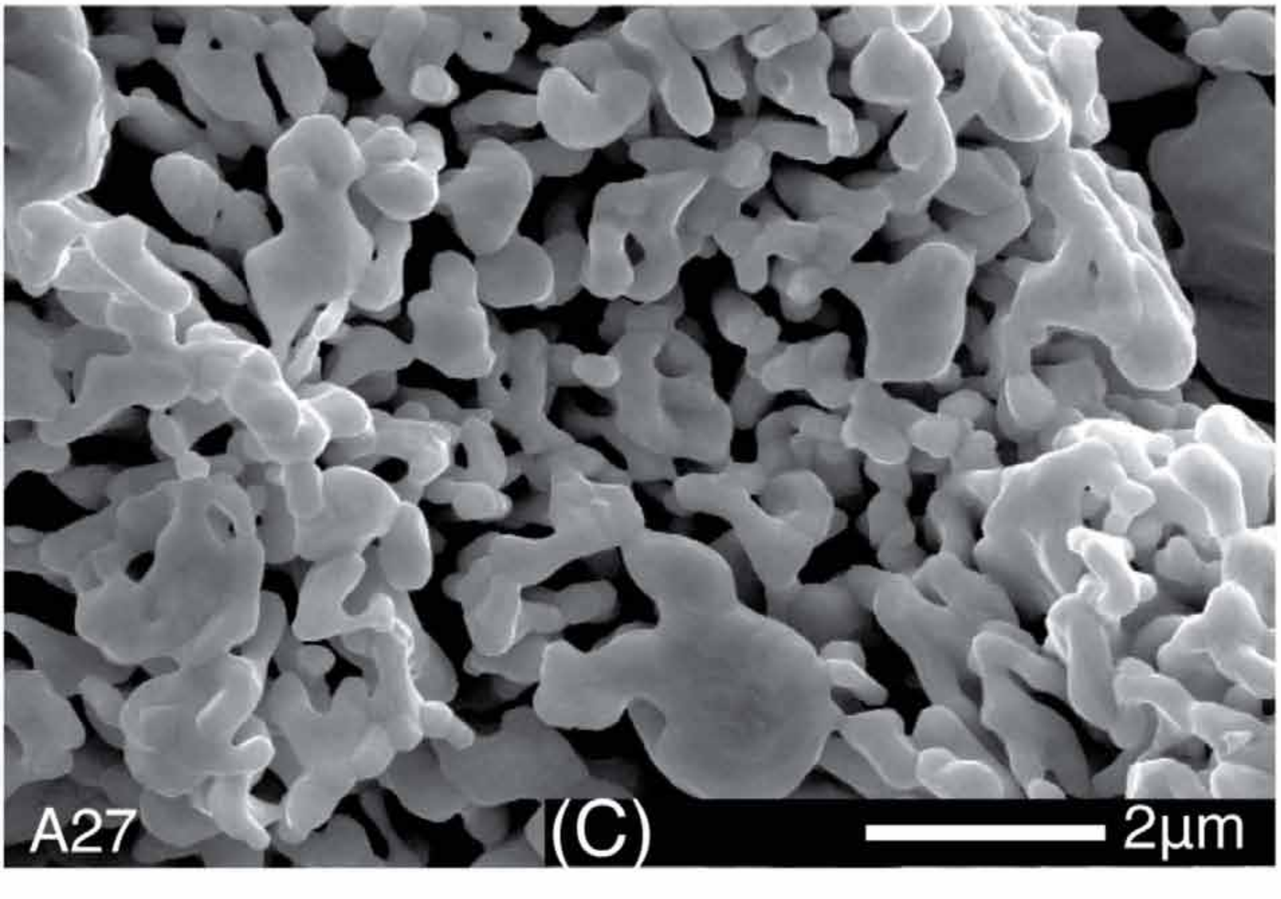
A27
(C)
2µm

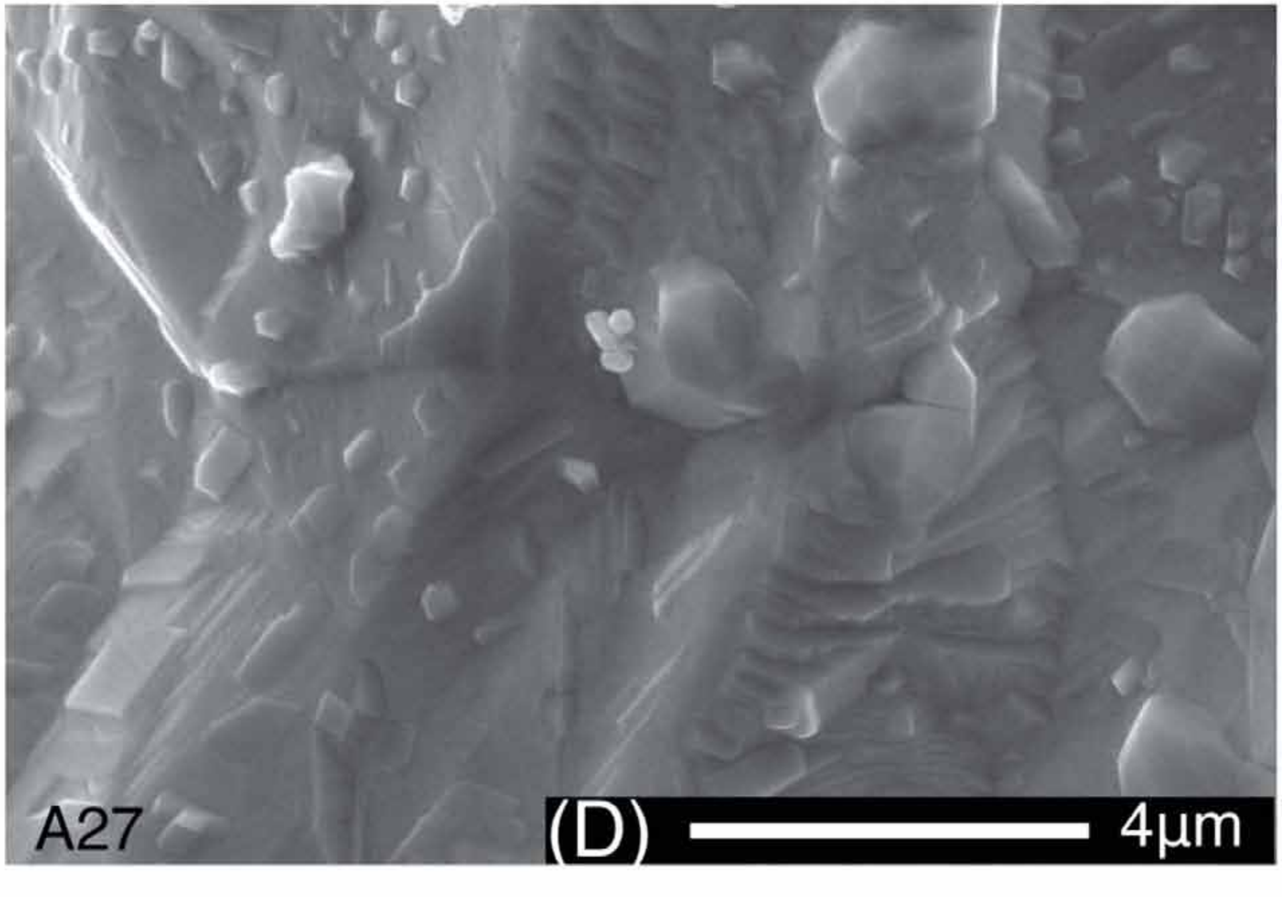
A27
(D)
4µm

(A) A28 10μm

(B) A28 10μm

Au-Ag alloy

Sylvanite

Petzite

Hessite

Calaverite-I

(C) A25 100μm

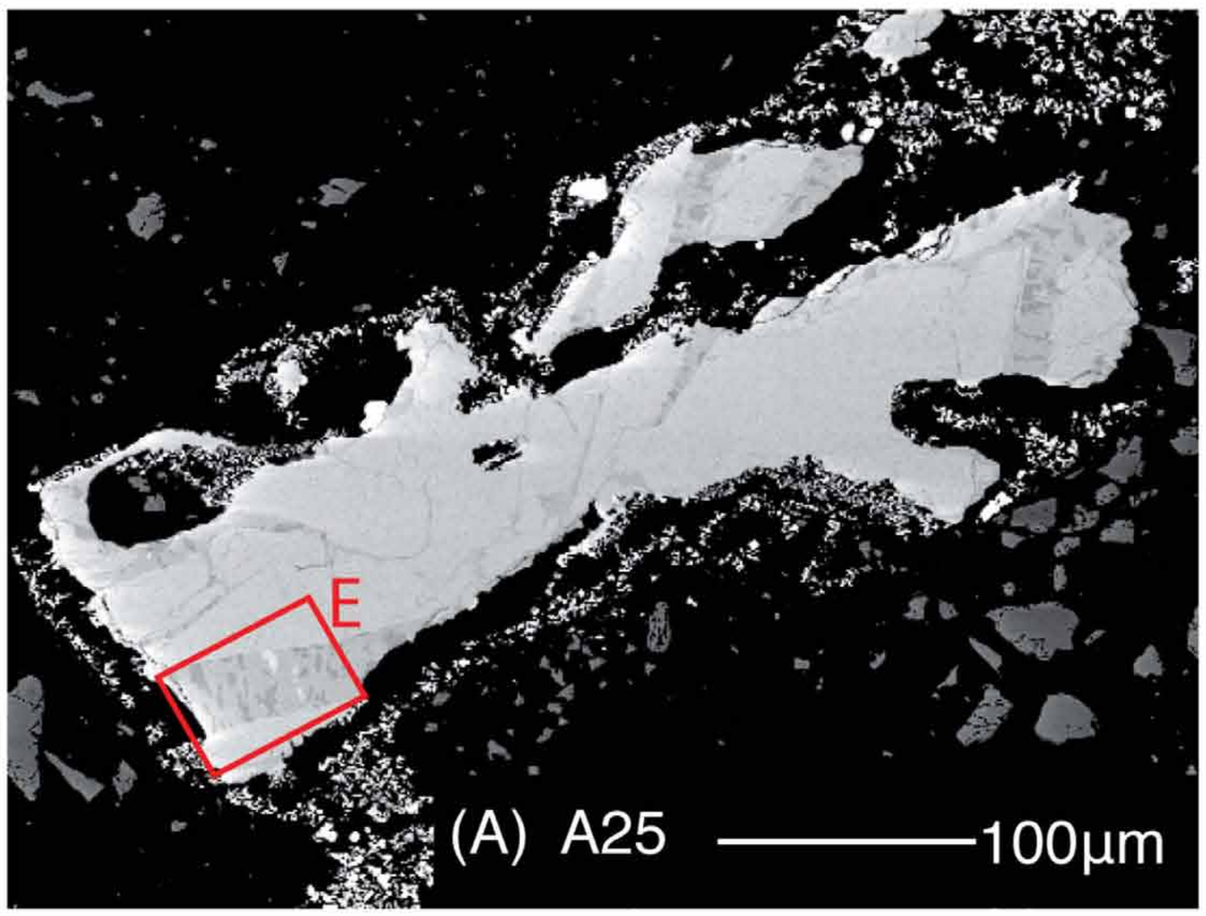
E
(A) A25
100µm

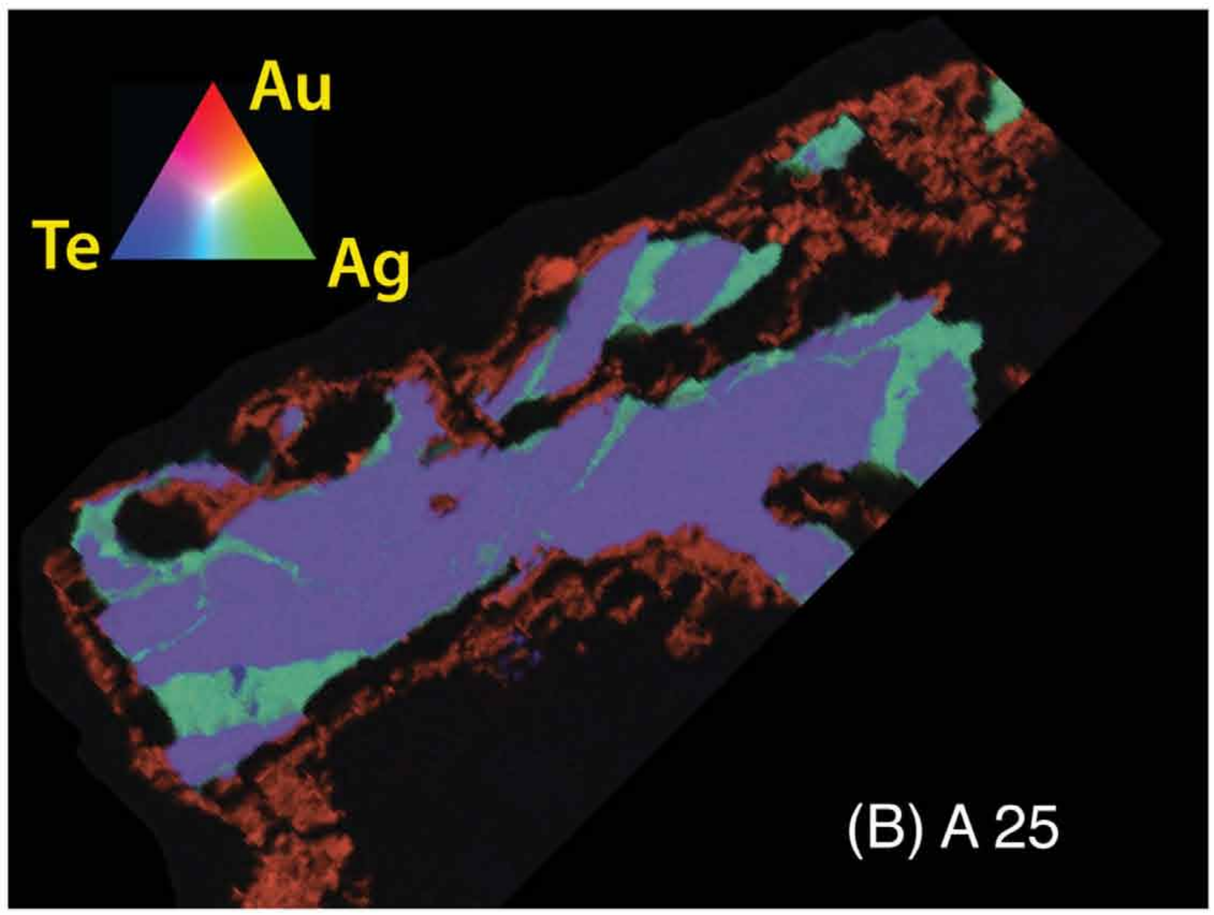
Au
Te
Ag
(B) A 25

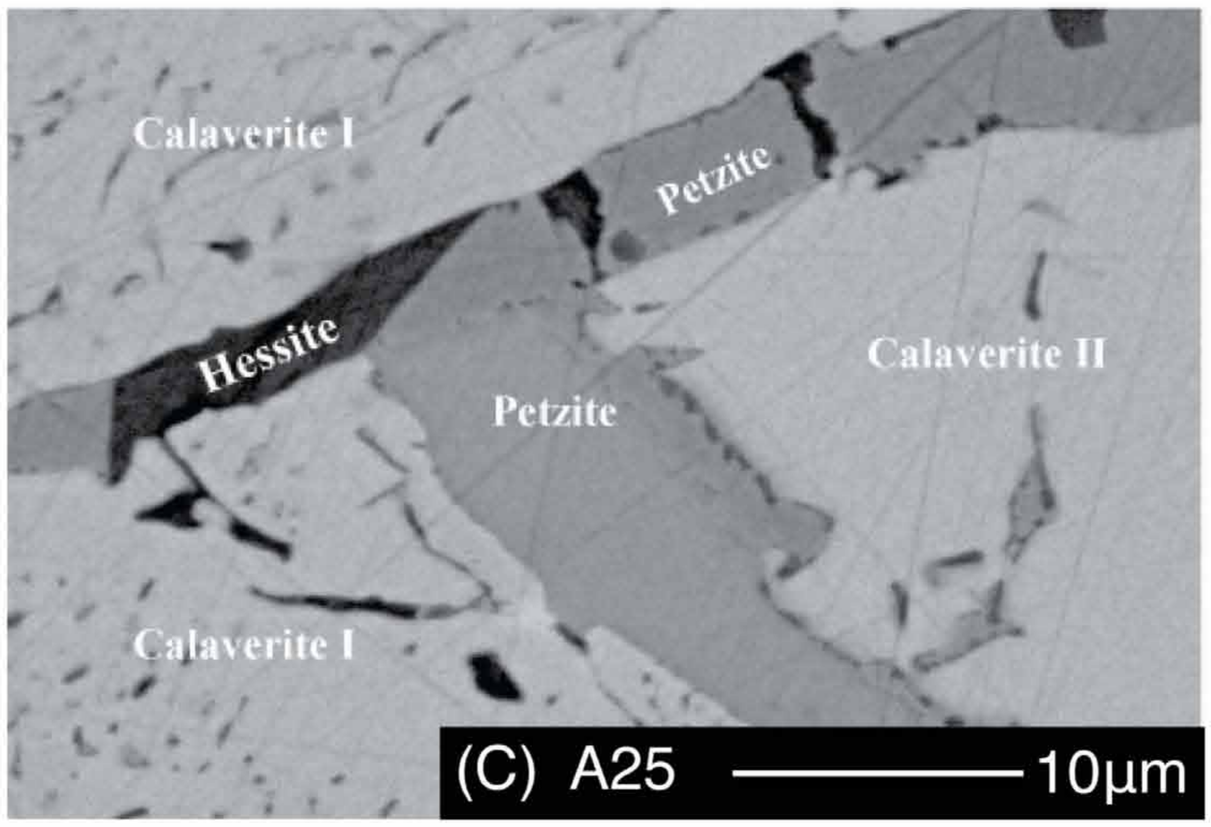
Calaverite I
Petzite
Hessite
Calaverite II
Petzite
Calaverite I
(C) A25
10µm

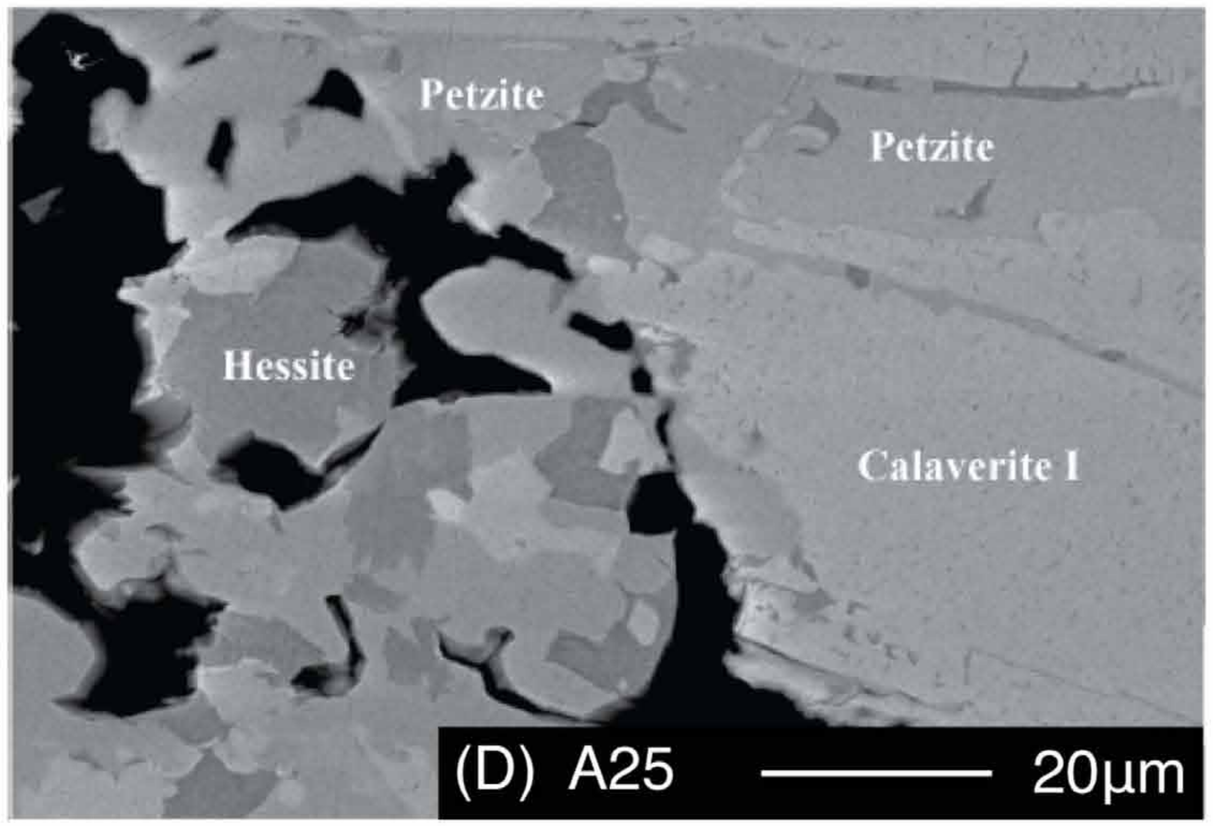
Petzite
Petzite
Hessite
Calaverite I
(D) A25
20µm

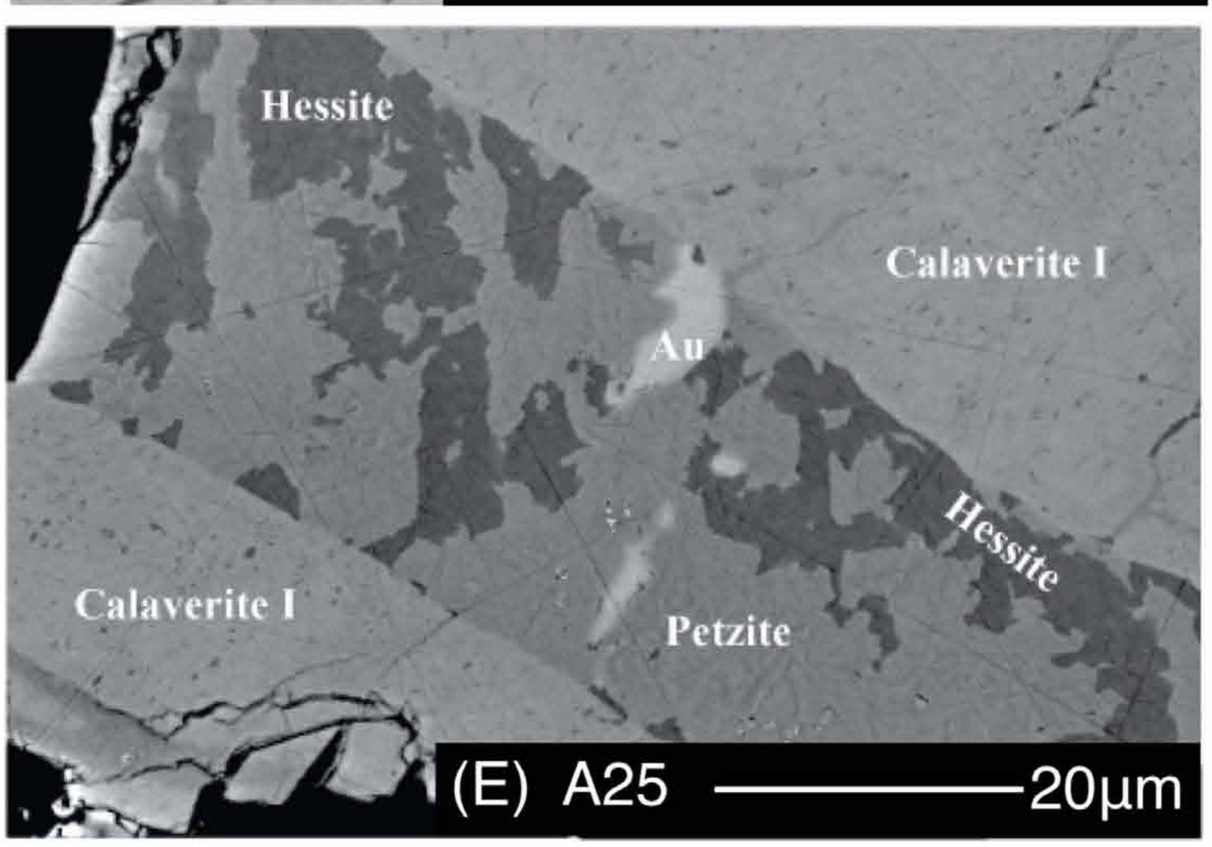
Hessite
Calaverite I
Au
Hessite
Calaverite I
Petzite
(E) A25
20µm

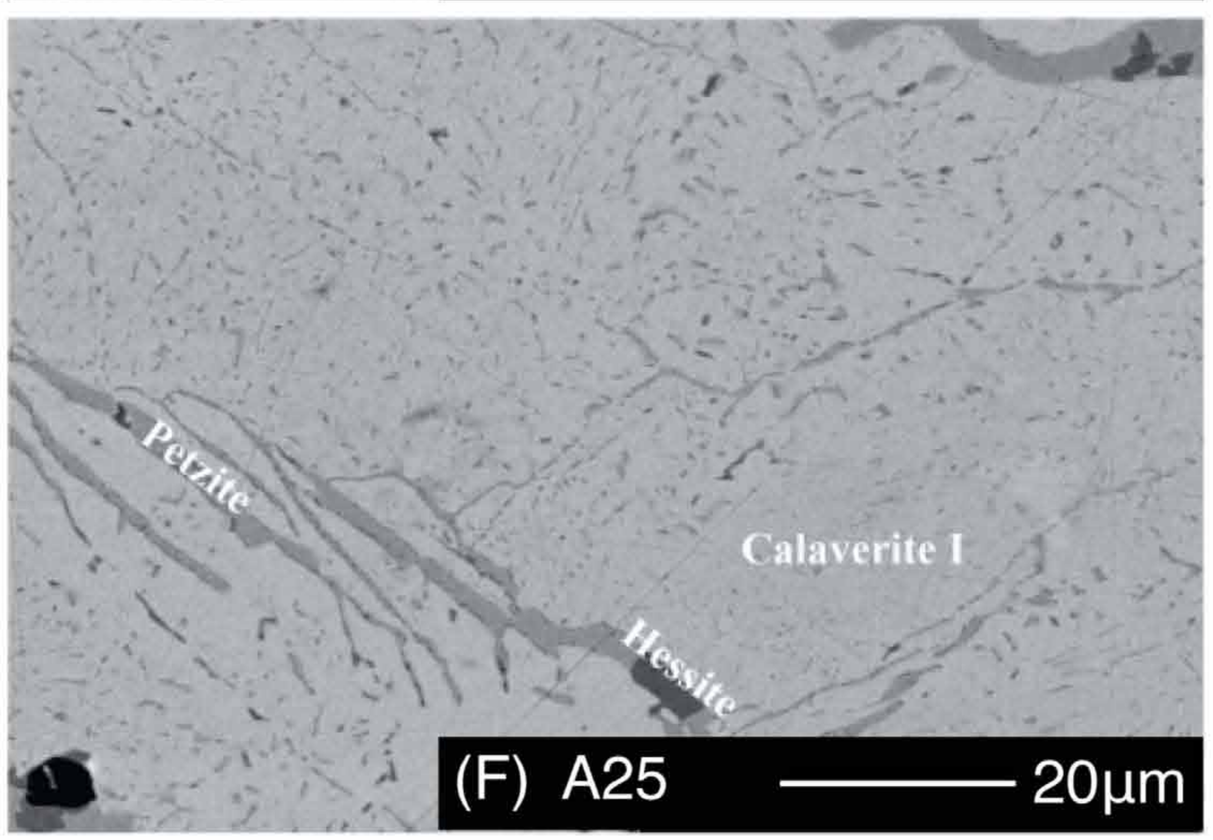
Petzite
Calaverite I
Hessite
(F) A25
20µm

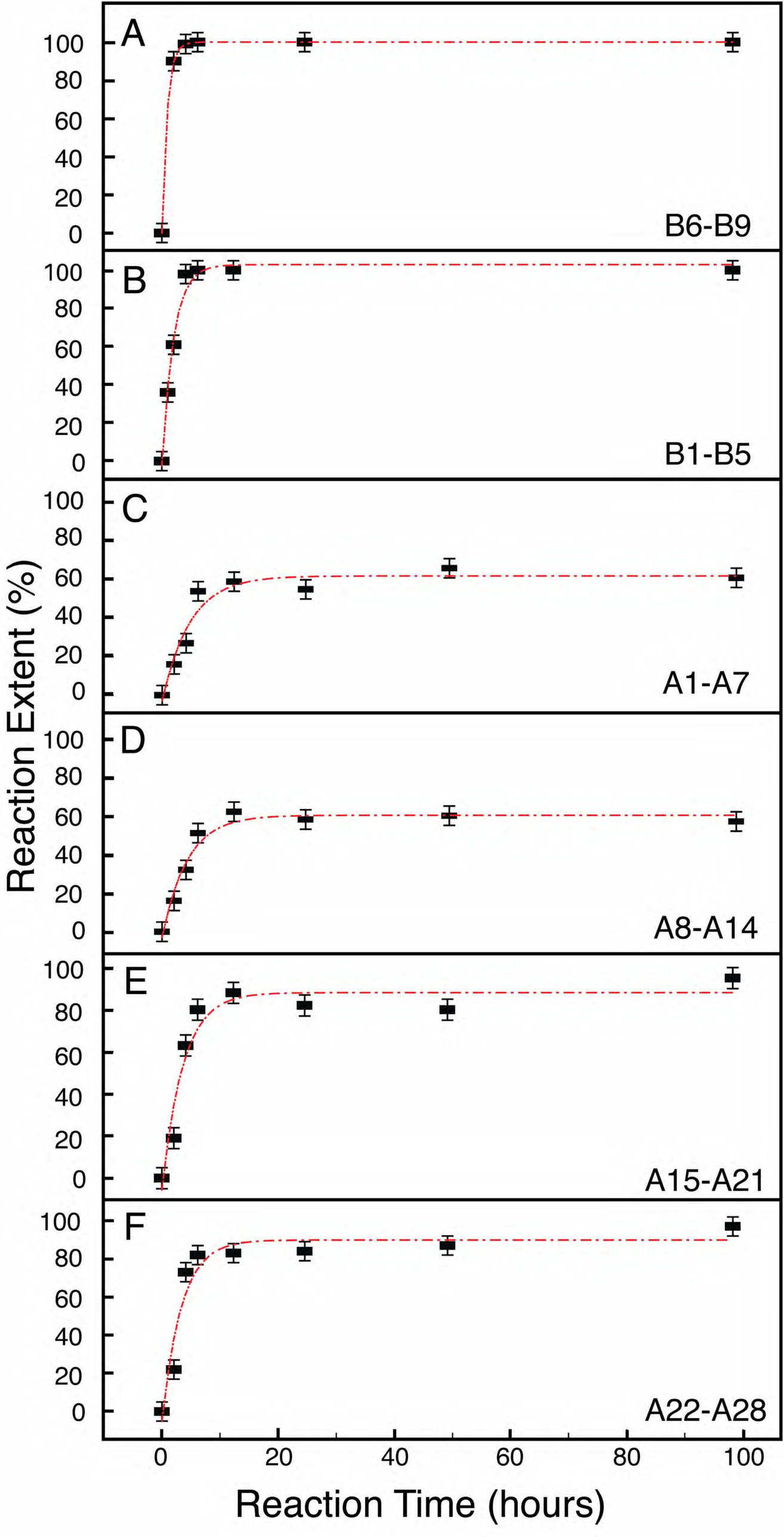
A
B6-B9
B
B1-B5
C
A1-A7
D
A8-A14
E
A15-A21
F
A22-A28
Reaction Extent (%)
Reaction Time (hours)
0
20
40
60
80
100

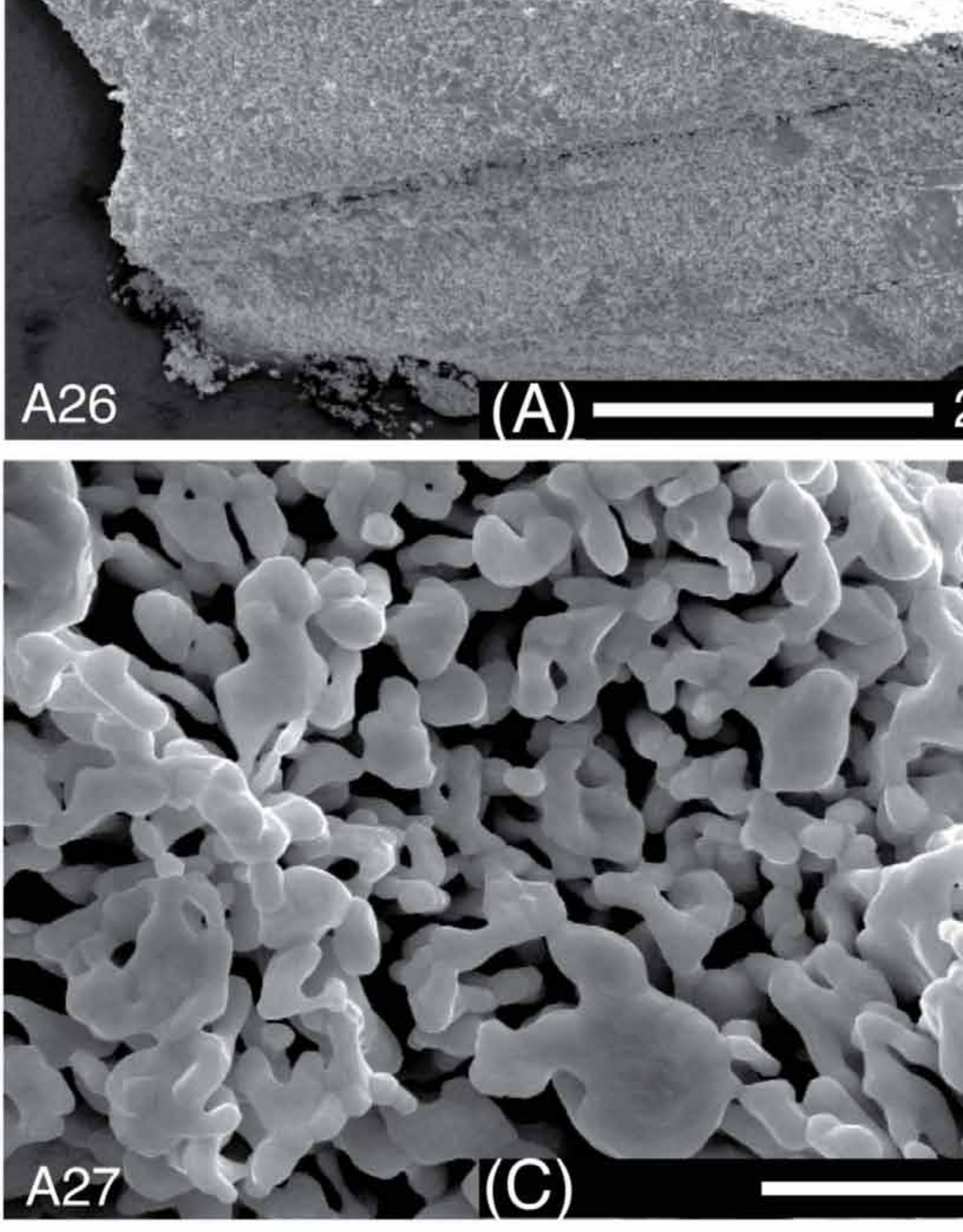
A26
(A)
A27
(C)

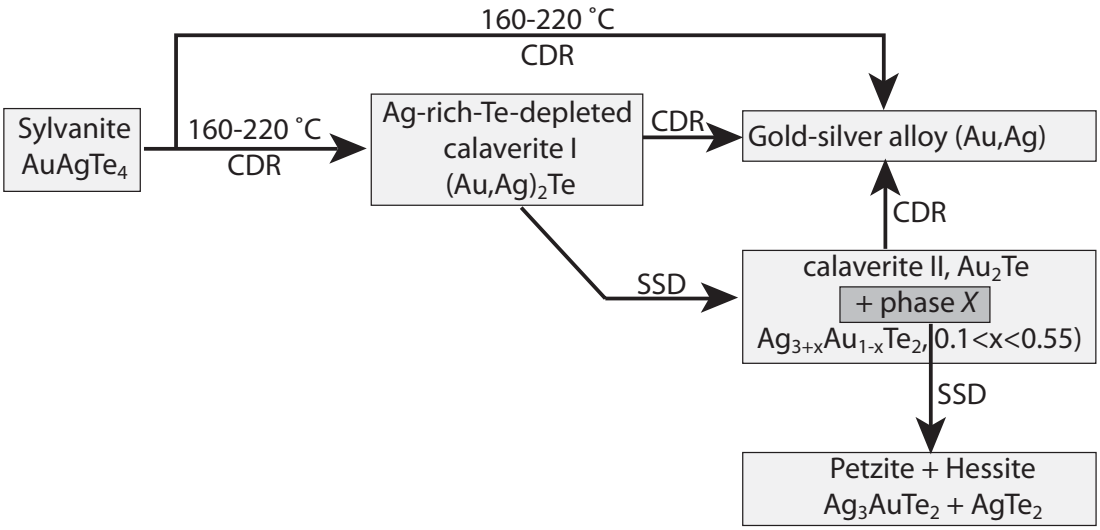
160-220 ˚C
CDR
Sylvanite
AuAgTe4
160-220 ˚C
CDR
Ag-rich-Te-depleted
calaverite I
(Au,Ag)2Te
CDR
Gold-silver alloy (Au,Ag)
CDR
SSD
calaverite II, Au2Te
+ phase X
Ag3+xAu1-xTe2, 0.1<x<0.55)
SSD
Petzite + Hessite
Ag3AuTe2 + AgTe2

log Au [ppm]

A)

AuCl(aq)

AuClOH

$Au(OH)_2^-$

-2.3

-5

log fO_2(g)

pH

log Te [ppm]

B)

H_2TeO_3(aq)

$HTeO_3^-$

TeO_3^{2-}

H_2Te(aq)

HTe^-

Te_2^{2-}

P2

neutral

P7

B10

pH

log Ag [ppm]

C)

AgCl(aq)

$Ag(OH)_2^-$

-0.699

-4.6

pH

Saturation index (SI) for petzite

D)

-10

-5

-4

pH

Minerals

E)

tellurite

tellurite +silver

silver

all in solution

gold+tellurite

gold+ tellurite+silver

silver + gold

gold+tellurite+hessite

hessite + gold

calaverite + hessite

calaverite + hessite + gold

calaverite + hessite +tellurium

Hm

Mt

1% H_2

P2

neutral

P7

B10

pH

Minerals (petzite metastable)

F)

tellurite

tellurite+ silver

silver

all in solution

Au + tellurite

gold+tellurite +silver

silver + gold

Au + hessite +tellurite

gold+hessite

Au + petzite +tellurite

gold+petzite

calaverite + petzite +tellurite

gold+calaverite+petzite

calaverite + petzite

calaverite + petzite +tellurium

calaverite + petzite

pH

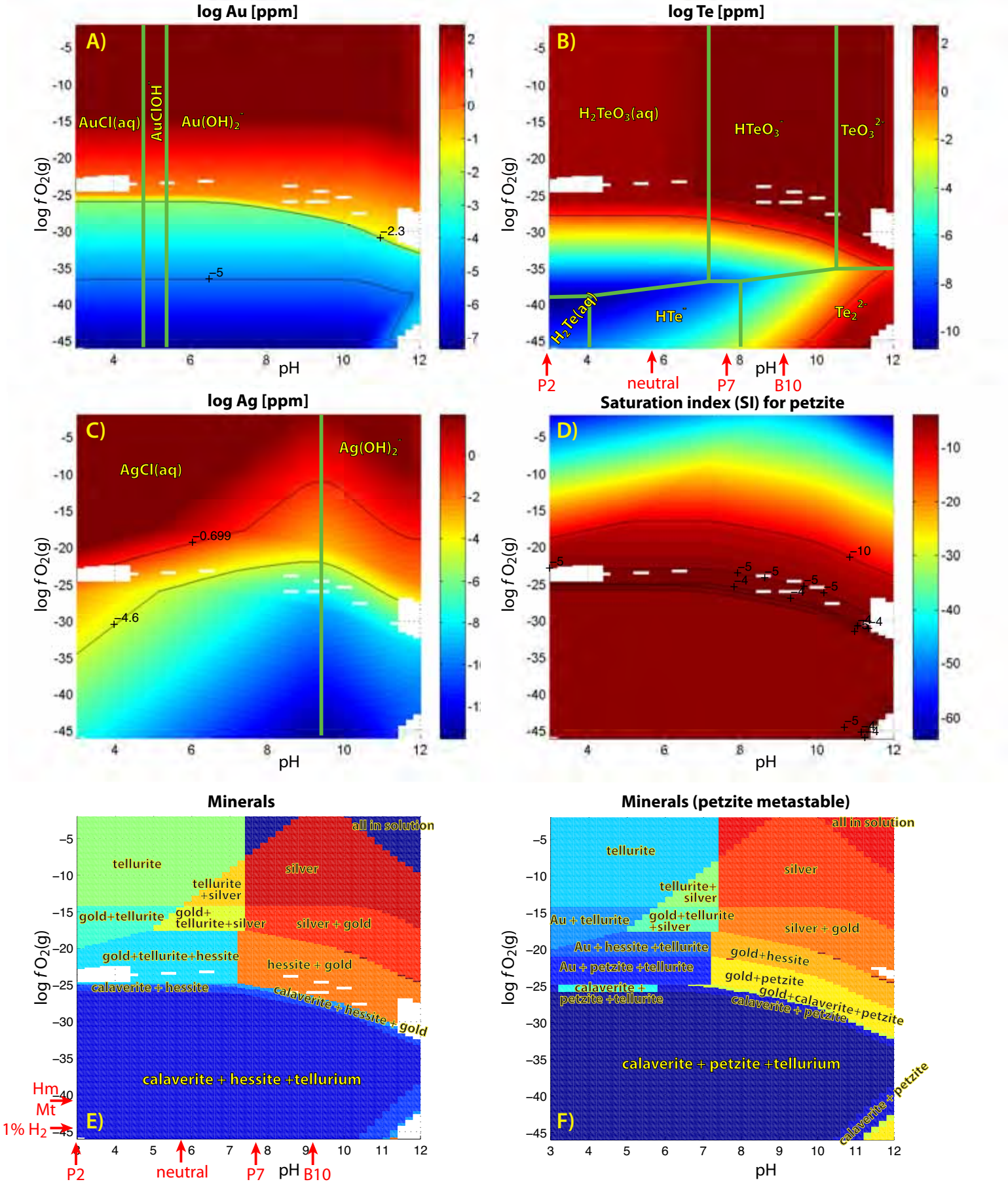
log Au [ppm]
A)
AuCl(aq)
AuClOH
Au(OH)2
-2.3
-5
log fO2(g)
pH
log Te [ppm]
B)
H2TeO3(aq)
HTeO3
TeO3 2-
H2Te(aq)
HTe
Te2 2-
P2
neutral
P7
B10
log Ag [ppm]
C)
AgCl(aq)
Ag(OH)2
-0.699
-4.6
Saturation index (SI) for petzite
D)
-10
-4.4
Minerals
all in solution
tellurite
silver
tellurite +silver
gold+tellurite
gold+ tellurite+silver
silver + gold
gold+tellurite+hessite
hessite + gold
calaverite + hessite
calaverite + hessite + gold
calaverite + hessite +tellurium
Hm
Mt
1% H2
E)
Minerals (petzite metastable)
tellurite
silver
tellurite+ silver
Au + tellurite
gold+tellurite +silver
silver + gold
Au + hessite +tellurite
gold+hessite
Au + petzite +tellurite
gold+petzite
calaverite + petzite +tellurite
gold+calaverite+petzite
calaverite + petzite
calaverite + petzite +tellurium
calaverite + petzite
F)